

Measurement of the Born-Forbidden Recoil Proton Normal Polarization in Electron-Proton Elastic Scattering

December 2, 2003

B. Anderson², D. Armstrong¹, R. Asatur¹³, T. Averett¹, E. Brash⁹, M. Finn¹, D. Gaskell¹¹, R. Gilman¹⁰, K. Griffioen¹, G. Huber⁹, S. Jin³, W. Kim³, D.J. Mack¹¹ (contact person), H. Mkrtchyan¹³, T. Navasardyan¹³, A. Opper⁷, C. Perdrisat¹, M. Pitt¹², V. Punjabi⁵, R. Segel⁶, N. Simicevic⁴, S.S. Stepanyan^{3,13}, V. Tadevosyan¹³, P. Ulmer⁸, J. Watson², S. Wells⁴, S.A. Wood¹¹

¹*College of William and Mary, Williamsburg, VA*

²*Kent State University, Kent, OH*

³*Kyungbok University, Taegu, Korea*

⁴*Louisiana Tech, Ruston, LA*

⁵*Norfolk State University, Norfolk, VA*

⁶*Northwestern University, Evanston, IL 60208*

⁷*Ohio University, Athens, OH*

⁸*Old Dominion University, Norfolk, VA*

⁹*University of Regina, Regina, Saskatchewan*

¹⁰*Rutgers University, Piscataway, NJ*

¹¹*TJNAF, Newport News, VA*

¹²*Virginia Polytechnic Institute, Blacksburg, VA*

¹³*Yerevan Physics Institute, Yerevan, Armenia*

Contents

| | | |
|----------|---|-----------|
| 1 | Executive Summary | 3 |
| 2 | Introduction | 5 |
| 2.1 | Helicity Amplitudes | 6 |
| 2.2 | Potential Scientific Impact | 8 |
| 2.2.1 | electric form factor of the proton | 8 |
| 2.2.2 | parity violating electron scattering | 9 |
| 2.2.3 | electroweak box diagrams | 10 |
| 2.2.4 | nuclear elastic form factors | 11 |
| 2.3 | Real Part of \mathcal{M}_2 | 12 |
| 2.3.1 | the cross section, σ | 12 |
| 2.3.2 | the beam charge asymmetry, R^\pm | 13 |
| 2.4 | Imaginary Part of \mathcal{M}_2 | 15 |
| 2.4.1 | the transverse beam spin asymmetry, A_N^e | 15 |
| 2.4.2 | the normal polarization, P_N or A_N^T | 15 |
| 3 | The Experiment | 20 |
| 3.1 | Kinematics | 22 |
| 3.2 | Standard Equipment | 23 |
| 3.2.1 | Electron Spectrometer | 23 |
| 3.2.2 | Cryotarget | 24 |
| 3.2.3 | Electron Beam Polarimeter | 24 |
| 3.3 | Nucleon Polarimeter | 24 |
| 3.3.1 | Overview of Nucleon Polarimetry | 24 |
| 3.3.2 | Hardware | 26 |
| 3.3.3 | Alignment | 31 |
| 3.3.4 | Absolute Determination of P_N | 32 |
| 3.4 | False Asymmetries and Spin Precession | 32 |
| 3.4.1 | basic spin precession facts | 33 |
| 3.4.2 | Intrinsic False Asymmetries | 34 |
| 3.4.3 | Induced False Asymmetries | 36 |
| 3.5 | Backgrounds | 39 |
| 3.6 | Trigger and Data Acquisition | 40 |
| 3.7 | Deuterium Measurements | 41 |
| 3.7.1 | Exploratory Measurements on the Neutron | 41 |
| 3.8 | Errors | 42 |
| 3.8.1 | Random Errors | 42 |
| 3.8.2 | Systematic Errors | 42 |
| 4 | Relation to Other Experiments | 47 |
| 5 | Collaboration | 47 |

| | | |
|---|---------------------|----|
| 6 | Beam Request | 47 |
| 7 | Acknowledgements | 48 |
| A | Neutron Polarimetry | 54 |

Abstract

A “new” technique involving a solenoidal recoil polarimeter is proposed to measure the small, beam helicity-independent induced normal proton polarization (P_N) in $e + p$ elastic scattering. This observable is proportional to the imaginary part of the two-photon exchange amplitude, so the interpretation of the observed asymmetry in terms of two-photon exchange does not require a delicate kinematic separation. The combination of a magnetic spectrometer for electron detection with a recoil polarimeter in the scattering plane provides turn-key isolation of the elastic reaction, a high figure of merit, complete control of the phase of the physics signal to cancel instrumental asymmetries, and the potential for extension to neutron measurements. If current models are correct and P_N is of order 1%, non-zero measurements with significance on the order of 10σ are anticipated. We thus expect to provide very tight constraints on model-dependent calculations of two-photon exchange in the most important energy region for precision electroweak measurements on the nucleon.

1 Executive Summary

In an era of increasingly precise measurements of the interaction of electrons with nucleons and nuclei, the proper treatment of hadronic uncertainties in two-photon exchange may now be the weakest link in our use of QED as a tool to study strongly-interacting matter. We are proposing a measurement of the Born-forbidden normal proton polarization, P_N , in $e + p$ elastic scattering. This observable, which calculations suggest is of order 1% for multi-GeV beam energies, is directly related to the imaginary part of the two-photon exchange amplitude. Two-photon exchange effects are one possible solution to the “ G_E^p crisis”, may make significant contributions to γZ interference in parity-violating electron scattering, and will eventually help reduce the hadronic uncertainties in γW box diagrams in low-energy charged current reactions of fundamental interest.

For center of mass energies above pion threshold, there are large contributions from inelastic intermediate states which cause calculations to be highly model-dependent. Since neither the magnitude nor the kinematic dependencies of two-photon exchange effects are known, other precision measurements besides G_E^p derived from Rosenbluth separations could be affected outside their error bars. Exactly which experiments and in which kinematic regimes are most affected will undoubtedly be the subject of much discussion in our community over the next few years. The beam energies of our experiment will complement those of ongoing electroweak measurements of (quasi-)elastic scattering and thus help constrain this model dependence.

Since all previous measurements of P_N and A_N using conventional FPP and normally-polarized targets are consistent with zero, we plan to use a new technique with a superconducting solenoid magnet to precess the proton spin by an angle χ

and cancel most instrumental asymmetries. The physics signal can be extracted by its clear $\cos(\phi + \chi)$ dependence. This technique is well-suited to the relatively small asymmetries expected in the energy range of 0.5-3 GeV, a range which is critical for many precision electroweak measurements. It also allows one to vary the importance of various intermediate inelastic contributions, from the Δ resonance to well above the resonance region. Anticipated statistical and systematic errors vary with kinematic setting, but are at the 0.1% level. If P_N is only half the predicted magnitude, we will still be able to make highly significant measurements.

Our proposed measurement of P_N is complementary to measurements which are sensitive to the real part of the two-photon amplitude. Our proposal is also complementary to measurements of the transverse beam spin asymmetry with G^0 -style apparatus since these involve an orthogonal set of helicity amplitudes.

Exploratory measurements of P_N in quasi-elastic $e + p$ and $e + n$ scattering on the deuteron will also be made to study the interplay of strong- and electromagnetic final state interactions, employing strong-FSI calculations by Arenhoevel and our own free- and bound-proton measurements. For deuterium, the predicted rapid decrease with Q^2 of P_N due to strong-FSI suggests it will be possible to make significant measurements of two-photon exchange effects on the neutron.

Finally, the proposed measurement has broader implications for field theory and for tests of the consistency of the Standard Model. The interpretability of precision electroweak measurements depends in part on the ability to assign uncertainties to two-boson exchange contributions (the so-called "box diagrams"). Hadronic uncertainties arising from long-distance scale QCD are present in both the γZ and γW box diagrams. Because the γW box diagrams are $O(\alpha)$ radiative corrections to nuclear β decay, they affect precision tests of the unitarity of the CKM matrix. Although the term is small, and the errors have been conservatively estimated, no dynamical calculation has been made. The development of an adequate model of $\gamma\gamma$ box diagrams (also known as two-photon exchange), thoroughly tested by experiment, could provide the necessary guidance for reducing hadronic uncertainties in γZ and γW box diagrams where independent tests are almost impossible.

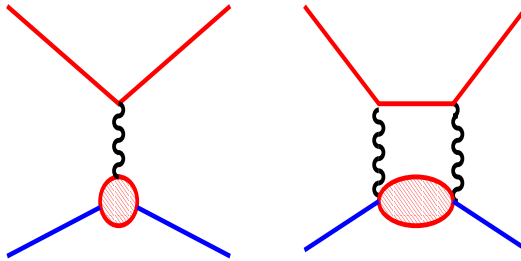


Figure 1: The dominant two-photon exchange effect results from the interference of the above one- and two-photon exchange diagrams.

2 Introduction

Electron scattering experiments typically probe nucleons and nuclei using Quantum Electrodynamics (QED) as an interpretational tool. At modern electron accelerator facilities, beams are pure, monoenergetic, intense, and with extremely low emittance. Since the electron is a point particle, with a coupling to photons significantly less than 1, the real or virtual emission of photons is calculable to high order. Many experiments on the nucleon or light nuclei can be interpreted with good precision using single photon exchange (*ie*, the Born approximation), provided so-called radiative corrections account for a second real or virtual photon.[1] No other community in nuclear or particle physics can boast this combination of beam quality and interpretability in its probe of choice. The scientific community is well-served by pushing these facilities to their limits.

However, electron scattering is not simply QED. The non-pointlike structure of nucleons and nuclei, and the existence of excited states of the strong Hamiltonian, means that electromagnetic form factors[2, 3] (or *effective* charge and magnetic moments) are already needed to describe the results in single photon approximation. This is of course a feature rather than a bug, because these useful phenomenological form factors are convenient meeting places between theory and experiment, reflecting the ability of electromagnetic currents in the target to absorb the virtual photon's energy and momentum (with the trivial Mott cross section effects removed).

Figure 1 shows a single photon exchange diagram as well as a box diagram in which the proton absorbs one photon, propagates in its ground or excited state, then exchanges a second photon with the electron. Although the *net* four-momentum transfer to the target in both cases is well-defined, $Q^2 \equiv -q^2$, in the box diagram the momenta of the two photons is integrated over all accessible values of q_1 and q_2 subject to the constraint that $q_1 = q_2 - q$. The amplitude corresponding to intermediate states with an elastic proton can be calculated model-independently, however, the amplitude arising from intermediate excited states (including both resonances and the non-resonant continuum) cannot. Model dependence necessarily

arises because simplifications have to be made. Due to interference between one- and two-photon exchange amplitudes, two-photon exchange corrections make their presence felt roughly a factor of α below one-photon exchange. However, the dynamical effects already mentioned could enhance this. Thus, in practical terms, **the most serious ambiguities in the interpretation of electron scattering data arise from the model-dependent intermediate inelastic states (*i.e.*, dispersive corrections) from the two-photon box diagrams as in Figure 1.**

It is hard to improve on the following description of the issue of two-photon exchange from Werthamer and Ruderman[4]:

Other corrections to the Born Approximation involve the exchange of more than one photon between the electron and the nucleon. Part of this represents the correction for multiple scattering of the electron by the static electric and magnetic fields of the nucleon. These would be included by explicitly solving the Dirac equation for the electron rather than using the Born approximation. The rest of the many-photon exchange contribution depends upon the dynamical structure of the nucleon charge and moment distribution and cannot be calculated even if the conventional form factors are known.

2.1 Helicity Amplitudes

To understand the complementary relationship between the different possible observables which are sensitive to two-photon exchange, and their relationship to ordinary observables like the cross section, we must go beyond the convenient but vague notation of $Real(\mathcal{M}_2)$ and $Im(\mathcal{M}_2)$ and use the more formal language of helicity amplitudes.

For a binary scattering of two spin-1/2 particles, with the spin projection along the momentum vector (*i.e.* the helicity) labelled by $\lambda_1, h_1, \lambda_2, h_2$,

$$e(1/2, \lambda_1) + p(1/2, h_1) \rightarrow e(1/2, \lambda_2) + p(1/2, h_2) \quad (1)$$

there are $2^4 = 16$ helicity amplitudes of the type $T_{\lambda_1 h_1}^{\lambda_2 h_2}$. Under the assumption of parity conservation this reduces to 8 amplitudes, and assuming time reversal invariance this finally reduces to a “mere” 6 complex amplitudes denoted $A1, A2, \dots, A5, A6$. [5] The first three amplitudes conserve lepton helicity

$$A1 \equiv T_{1/2, 1/2}^{1/2, 1/2}, \quad A2 \equiv T_{1/2, -1/2}^{1/2, -1/2}, \quad A3 \equiv T_{1/2, -1/2}^{1/2, 1/2} \quad (2)$$

while the last three amplitudes require a lepton helicity flip

$$A4 \equiv T_{1/2, 1/2}^{-1/2, 1/2}, \quad A5 \equiv T_{1/2, 1/2}^{-1/2, -1/2}, \quad A6 \equiv T_{1/2, -1/2}^{-1/2, 1/2} \quad (3)$$

The above expressions are reasonably general. However, if we now identify particle e with the electron, p with the proton, and work in the limit that $\gamma \gg 1$ then the electron helicity is almost a good quantum number and electron helicity-flip transitions are suppressed by $m/E = 1/\gamma$. In the following, it is critical to

realize that, since $A4, A5, A6$ require an electron helicity-flip, these amplitudes are relatively miniscule compared to $A1, A2, A3$.

Using the simplified notation $Ai^2 \equiv Ai^*Ai$, with N a kinematic factor, the parity-conserving observables are: the cross section,

$$\sigma = N(A1^2 + A2^2 + 2A3^2 + 2A4^2 + A5^2 + A6^2) \simeq N(A1^2 + A2^2 + 2A3^2) \quad (4)$$

the longitudinal polarization ($\hat{L} \equiv \frac{\vec{P}_e - \vec{P}_{e'}}{|\vec{P}_e - \vec{P}_{e'}|}$)

$$P_L = \frac{N}{\sigma}(A1^2 - A2^2 + A5^2 - A6^2) \simeq \frac{N}{\sigma}(A1^2 - A2^2) \quad (5)$$

the polarization normal to the scattering plane ($\hat{N} \equiv \frac{\vec{P}_e \times \vec{P}_{e'}}{|\vec{P}_e \times \vec{P}_{e'}|}$), or the asymmetry for scattering from a normal polarized target,

$$P_N = A_N^T = \frac{2N}{\sigma} \text{Im}[(A1 + A2)A3^* + A4(A6^* - A5^*)] \simeq \frac{2N}{\sigma} \text{Im}[(A1 + A2)A3^*] \quad (6)$$

the ‘‘sideways’’ polarization ($\hat{T} \equiv \hat{L} \times \hat{N}$)

$$P_T = \frac{2N}{\sigma} \text{Re}[(A1 + A2)A3^* + A4(A6^* - A5^*)] \simeq \frac{2N}{\sigma} \text{Re}[(A1 + A2)A3^*] \quad (7)$$

and finally the transverse beam spin asymmetry,

$$A_N^e = \frac{2N}{\sigma} \text{Im}[fnc(A1, A2, A3, A4, A5, A6)] \ll \alpha \quad (8)$$

For a polarized beam, the in-plane polarizations P_T and P_L are allowed in one-photon exchange approximation.[6] Like the cross section, they contain different combinations of the real part of the two-photon amplitudes as well as large one-photon exchange backgrounds. Presumably, existing measurements of FPP P_T/P_L and Rosenbluth separation cross sections already constrain the real part of the two-photon exchange amplitude, but there are plans to tighten these constraints.[7, 8]

The beam charge asymmetry, A^\pm (*i.e.*, the positron-electron cross section difference asymmetry) would be of great interest because, although it has the same helicity amplitude dependences as σ , the single-photon exchange backgrounds cancel. This observable would tell us *exactly* what role two-photon exchange effects were playing in Rosenbluth separations. However, evidence for significantly non-zero effects is unconvincing (see Figure 2 and Ref. [9]), and there is currently no facility available for improved measurements.

The transverse beam spin asymmetry, A_N^e , is also free of large one-photon exchange backgrounds and is sensitive to the imaginary part of the two-photon exchange amplitude. However, from the above discussion it is expected to be small (confirmed by experiment in [10]) and contains the otherwise completely unconstrained amplitudes $A4, A5$, and $A6$. Thus, A_N^e should perhaps best be thought of

as a probe of these exotic amplitudes. The combination of P_N and A_N^e measurements, because they both involve the imaginary part of the two-photon amplitudes, may make it possible to tightly constrain $A4 - A6$.

For an unpolarized (or helicity averaged) beam, P_T and P_L must vanish by parity conservation.¹ The only non-vanishing polarization is P_N , the polarization of the proton normal to the electron scattering plane. P_N must be zero in Born approximation since it corresponds effectively to a tree-level T-odd interaction such as $\vec{\sigma}_p \cdot (\vec{p}_e \times \vec{p}_{e'})$. A non-zero P_N can nevertheless be generated in a T-invariant manner by the interference of the real one-photon amplitude and the imaginary part of the two-photon amplitude.

Given our current inability to make measurements of A^\pm , the observable P_N is perhaps most promising for providing new information about two-photon exchange effects in electron scattering. Like, A_N^e , it is proportional to the imaginary part of two-photon exchange amplitudes. However, P_N is dominated by the same $A1 - A3$ amplitudes which dominate in σ , P_L , and P_T .

2.2 Potential Scientific Impact

2.2.1 electric form factor of the proton

Although an improved treatment of two-photon radiative corrections may be important for a wide range of precision electron-scattering measurements, one hopes that the worst-case scenario has already been encountered in the form of the “ G_E^p crisis”. The G_E^p crisis, simply put, is the significant discrepancy between measurements of G_E^p derived from precision Rosenbluth separations and those from the ratio of transverse to longitudinal recoil proton asymmetries made with a focal plane polarimeter[11]. The fact that the discrepancy becomes significant above $Q^2=1$, just as the electric contribution to the cross section ratio $\epsilon(G_E^p)^2/\tau(G_M^p)^2$ becomes $O(10\%)$ (while the P_T/P_L is still $O(1)$) is suggestive that the problem lies largely in the Rosenbluth separations. Recent Rosenbluth separations employing the $^1H(e, p)e$ reaction have confirmed the trend of the older $^1H(e, e')p$ measurements but with much smaller systematic and statistical uncertainties.[12] This is consistent with, but not proof of, a two-photon exchange explanation since the reaction has the same internal radiative corrections whether one is detecting an electron or a proton. Furthermore, it is very unlikely that so many experimental groups, using different techniques, would all make such large systematic errors in the same direction. This suggests that the problem lies in our interpretational tools, *i.e.* the single photon approximation plus Mo and Tsai radiative corrections. Thus, the “ G_E^p crisis” is not limited to the electric form factor of the proton or delicate Rosenbluth separations, but is a crisis of credibility for the entire electron scattering community.

¹The smallest asymmetry we will measure is 0.05%, or 500 ppm, which is more than an order of magnitude larger than the size of parity-violating asymmetries expected at our low Q^2 .

2.2.2 parity violating electron scattering

The amplitude due to internal soft two-photon exchange is infra-red divergent and cancels with external soft-photon emission on one fermion leg. Thus, two-photon exchange has not been thought to play any role in parity-violating electron scattering. However, Afanasev has pointed out that the factorizability arguments used for soft photons break down in the presence of hard two-photon exchange.[13] Although quantitative estimates are still in progress, it is clear that the standard picture of γZ interference must break down at order α when hard two-photon exchange is considered.

The parity-violating asymmetry is proportional to the γZ interference term

$$A_{PV} \propto \text{Real}(\mathcal{M}_{EM}^* \mathcal{M}_Z) = \text{Real}(\mathcal{M}_{EM}) \mathcal{M}_Z \quad (9)$$

where in \mathcal{M}_Z only the parity-violating terms $Axial^e \times Vector^h$ and $Vector^e \times Axial^h$ contribute, and we have made use of the fact that \mathcal{M}_Z is real. Thus, *only the real part of the electromagnetic amplitude contributes to parity-violation*, a fact which will be implicit in the following discussion. Since $\mathcal{M}_{EM} = \mathcal{M}_{1\gamma} + \mathcal{M}_{2\gamma}$, we can isolate the two-photon contribution and express it as the sum of (parity-conserving!) vector and axial-vector electromagnetic amplitudes using a Fierz transformation²:

$$A_{PV} \propto \mathcal{M}_{2\gamma} \mathcal{M}_Z = (\mathcal{M}_{2\gamma}^V + \mathcal{M}_{2\gamma}^A)(\mathcal{M}_Z^{AeVh} + \mathcal{M}_Z^{VeAh}) \quad (10)$$

Expanding, we find

$$A_{PV} \propto \mathcal{M}_{2\gamma}^V \mathcal{M}_Z^{AeVh} + \mathcal{M}_{2\gamma}^V \mathcal{M}_Z^{VeAh} + \mathcal{M}_{2\gamma}^A \mathcal{M}_Z^{AeVh} + \mathcal{M}_{2\gamma}^A \mathcal{M}_Z^{VeAh} \quad (11)$$

These are heuristic expressions since the important Q^2 and ϵ dependencies have been omitted. The axial and vector couplings of the Z to the electron are 1 and $(1 - 4 \sin^2 \theta_W)$, respectively. The latter term is $\ll 1$, so it is useful to make this dependence explicit using $\mathcal{M}_Z^{AeVh} \equiv \mathcal{M}_Z^{Ae} \mathcal{M}_Z^{Vh}$ and $\mathcal{M}_Z^{VeAh} \equiv \mathcal{M}_Z^{Ve} \mathcal{M}_Z^{Ah}$

$$A_{PV} \propto \mathcal{M}_{2\gamma}^V \mathcal{M}_Z^{Vh} + \mathcal{M}_{2\gamma}^V (1 - 4 \sin^2 \theta_W) \mathcal{M}_Z^{Ah} + \mathcal{M}_{2\gamma}^A \mathcal{M}_Z^{Vh} + \mathcal{M}_{2\gamma}^A (1 - 4 \sin^2 \theta_W) \mathcal{M}_Z^{Ah} \quad (12)$$

The first two terms have the familiar structure of the standard expression for γZ interference, in which contributions due to the axial nucleon form factor remain suppressed. The last two terms are rather unusual in that they involve $\mathcal{M}_{2\gamma}^A$. Assuming the effect is $O(\alpha)$, it may represent a large *relative* modification to the axial strength in a region where it is otherwise expected to be small, such as forward angles. For example, in the forward kinematics of the JLab Q_{weak}^p proposal[14], a fractional change in the axial strength of $O(\alpha)$ would represent a *relative* change of 15%. This is not a problem for the Q_{weak}^p experiment since the proposal assumed a

²This is the same reason that the handbag diagram in GPD's gives access to information about axial structure.

large 25% uncertainty on G_A^e . However, a detailed calculation should be performed since dynamical effects could alter this simple estimate.

To summarize, the major effect of two-photon exchange on parity violating electron scattering may be to make a small absolute change, but large in relative terms, in the amount of axial strength at forward electron angles.[13]. As our community attempts to make increasingly precise measurements of parity-violating asymmetries in its search for strange quark effects, physics beyond the Standard Model, etc., it becomes increasingly important that the formalism be accurate enough to fulfill these tasks. Although this issue has been raised only very recently by Afanasev and has not been presented even in preprint form, it will receive increasing attention. A crucial input to the calculations will be constraints on $Re\mathcal{M}_2$ which can be obtained model-dependently from the measurements of P_N proposed here.

2.2.3 electroweak box diagrams

Precision electroweak measurements allow the low energy community to make competitive searches for physics beyond the Standard Model far below the TeV scale needed to (potentially) put new particles on their mass shell for direct detection. Discovery of the exchange of “new” bosons even more massive than the Z or W (with correspondingly super-weak interactions) would require that one be able to distinguish between measurements which are consistent with the Standard Model and those which are not. This essential criterion, interpretability, is limited by uncertainties in the calculation of higher-order effects which, like the two-photon exchange process, begin at order α . In spite of the appearance of axial couplings and short distance scale in the electroweak case, there is a clear analogy between the $\gamma\gamma$ box diagrams and the γZ and γW box diagrams.

In radiative corrections to the weak charge of the proton, charge renormalization processes (*e.g.* γZ mixing) are particularly important. Fortunately, these diagrams can be related to $e^+e^- \rightarrow h\bar{h}$ via dispersion relations. But there are no data which similarly constrain the γZ , ZZ , and WW box diagrams which are obviously more closely related to the thrust of this proposal. In the case of the ZZ and WW box diagrams, the intermediate proton momenta are of order M_Z or M_W and can be treated perturbatively with modest uncertainties.[15] The γZ box diagrams, however, have important contributions from long distance scales and in principle it is necessary to include the intermediate excited states of the proton such as those to which the present proposal is sensitive. For the proton case, Erler *et al.* [17] found that, while the hadronic uncertainties in the γZ box diagrams are relatively large (of order 100%), a factor of $1 - 4\sin^2\theta_W$ helps reduce the net uncertainty on the Standard Model prediction of $Q_{weak}(proton)$ to less than 1%. Thus, a significant improvement in the uncertainties of the long range contributions to the γZ box diagrams is not expected to affect the interpretability of a future 3%-4% $Q_{weak}(proton)$ measurement.[14] In atomic parity violation experiments, the γZ contribution to the overall uncertainties is smaller because the weak charge of the neutron has no

$1 - 4 \sin^2 \theta_W$ suppression.[16]

By contrast, the γW box diagrams in nuclear beta decay are *not* suppressed by a factor of $1 - 4 \sin^2 \theta_W$, hence the long range contributions from intermediate proton excited states may be a more significant source of uncertainty.[17] Nuclear (or neutron) beta decay is used to extract the CKM matrix parameter V_{ud} which, because of its relatively large size, is critical for precision tests of the unitarity of transformations between the known 3 families of quarks. The standard reference to radiative corrections in neutron beta decay[18] approximated the γW box contributions but did not do dynamical calculations. This was certainly appropriate in 1978, but a new generation of experiments which plan to measure neutron beta decay spin-momentum asymmetries at the 0.2% level[19] will require a better theoretical foundation. We believe that measurements of two-photon exchange, and the development of models to explain these measurements, are necessary steps in reducing the hadronic uncertainties associated with the γW box diagrams in beta decay. Once a model has been shown to work for $\gamma\gamma$ box diagrams, it can be extended (by including axial couplings among other things) to γW boxes. This would provide the first real basis for estimating the uncertainties in the γW box diagrams.

2.2.4 nuclear elastic form factors

There is little direct connection between the measurements of P_N in this proposal and nuclear elastic form factors. While P_N is sensitive to intermediate *nucleon* excited states, two-photon exchange effects in nuclei are presumably dominated by virtual *nuclear* excitations. However, we mention the topic for completeness since the recent experience with G_E^p may now cause the issue of two-photon exchange to be taken more seriously in high Q^2 nuclear elastic form factors.

Multiple scattering theory predicts that two-photon exchange will become relatively more important than one-photon exchange in nuclear elastic scattering at higher Q^2 due to the much faster fall off of the nuclear (as opposed to the nucleon) form factor.[20] Due to the interference between one- and two-photon exchange, Franco [21] predicted that two-photon exchange effects in elastic $e + d$ scattering could be approximately 10% at $Q^2 = 1.3$. (A more recent discussion of this issue is by Rekaló *et al.*[22]) Since the two-photon exchange amplitude in this case is largely imaginary, relatively large P_N or A_N effects may also be expected. Dispersive effects have been observed in careful measurements of the energy dependence of the ^{12}C elastic form factor in the first diffraction minimum.[23] The observed effects were an order of magnitude larger than predictions, which suggests that important physics (Δ excitations?) was left out of the calculations.

Although such two-photon exchange effects in nuclei are perhaps crucial for interpreting nuclear elastic form factors in certain regimes, the added complications of multiple scattering and intermediate nuclear inelastic excitations mean that such studies are unlikely to yield much insight into dispersive effects in elastic scattering *on the nucleon*. Because our focus is on improving our ability to make fundamen-

tal measurements on the nucleon, we will not touch again upon the rich topic of dispersive effects in nuclei.

2.3 Real Part of \mathcal{M}_2

Expanding the above approximate helicity amplitude expressions into one-photon and two-photon contributions by

$$A1 \equiv A1_1 + A1_2, \quad A2 \equiv A2_1 + A2_2, \text{ etc.} \quad (13)$$

and defining

$$\sigma \equiv \sigma_1 + \sigma_2 \quad (14)$$

it is easy to show, dropping terms of higher order, that

$$\sigma_1 = N(A1_1^2 + A2_1^2 + 2A3_1^2) \quad (15)$$

and

$$\sigma_2 = 2N(A1_1 \text{Re}(A1_2) + A2_1 \text{Re}(A2_2) + 2A3_1 \text{Re}(A3_2)) \quad (16)$$

where σ_2 must be real but not necessarily positive. The beam charge asymmetry, A^\pm , cancels the large one-photon exchange backgrounds and is $2\sigma_2/\sigma_1$.

Expanding the observables P_T and P_L into one- and two-photon contributions is not very illuminating. There are large one-photon exchange backgrounds, and the two-photon contributions have rather complicated interferences (in the numerator and the denominator) between the dominant amplitudes, $A1 - A3$. The ratio P_T/P_L is somewhat interesting both formally and experimentally because of the cancellation of factors of σ .

2.3.1 the cross section, σ

Naively, the relative size of two-photon exchange corrections should be $O(\alpha) = 1/137$. This expectation is roughly borne out by essentially model-independent calculations which only include the proton intermediate state.[24] However, contemporary with the work of Hofstadter and collaborators[3], there was already concern about potential enhancements caused by intermediate excited states. The issue was serious since, if the effect of the intermediate resonances was to enhance two-photon exchange by an order of magnitude, it would have made it impossible to accurately interpret electron scattering data above a few hundred MeV beam energy using the single photon exchange formalism of Rosenbluth.[2] Model-dependent estimates of the resonance contributions[25] showed that these effects were only a factor of several larger than the intermediate elastic proton contributions, yielding a net contribution to the differential cross section of roughly 1/2% for 400 MeV increasing to 1% at 1 GeV. Calculations such as these put the single photon exchange approximation on a reasonable $O(\alpha)$ footing for cross section measurements.

Given that it is extremely difficult to do absolute cross section measurements at the 1% level, this level of uncertainty in single photon exchange appears at first glance to be acceptable. Obviously, in analyses based on the single photon exchange

approximation, effects of this small magnitude are routinely being swept under the rug of phenomenological form factors. But the calculations by Drell *et al.*[25] predicted effects which were 1% at 1 GeV and increasing with energy. This begs the question of what happens in the range 1-50 GeV where many contemporary experiments are done. Furthermore, detailed study of two-photon exchange effects is justified by the potential impact on *precision* measurements which utilize the Q^2 , θ_{CM} , or ϵ dependence of cross sections predicted in Born Approximation. In such cases the final errors on the result may be significantly larger than 1%.

In a long-overdue re-examination of the effect of radiative corrections on precision L-T separations, Blunden *et al.*[46] found that the ϵ dependence of the two-photon exchange diagram has a significant effect on the extraction of G_E^p from delicate Rosenbluth separations at higher Q^2 . Although their calculation only included the intermediate electron-proton states, they were able to account for nearly half the discrepancy between Rosenbluth separations and FPP measurements. It is far too early to declare victory since inelastic intermediate states have not yet been included; previous calculations for the e^+e^- cross section difference found that the inelastic contributions were somewhat larger and could even have opposite sign.[27] It is not inconceivable that the next generation of improved calculations of two-photon exchange effects on Rosenbluth separations could make the G_E^p crisis even worse. However, the lesson to be taken from this is that using Mo and Tsai radiative corrections and the traditional Rosenbluth formula is insufficient for delicate L-T separations.³

2.3.2 the beam charge asymmetry, R^\pm

In this section we define R^\pm to be the ratio of the e^+p/e^-p elastic scattering cross sections. A measurement of R^\pm is sensitive to the *real* part of the two-photon exchange amplitude, $\simeq 1 + 4Re(\mathcal{M}_2)/\mathcal{M}_1$. Similarly, it can be shown that the beam charge asymmetry, $A^\pm \equiv \frac{\sigma^+ - \sigma^-}{\sigma^+ + \sigma^-} \simeq 2Re(\mathcal{M}_2)/\mathcal{M}_1$.

Greenhut [27] calculated both the elastic and inelastic intermediate state contributions to R^\pm . The inelastic part of the model was fitted to a limited set of Compton scattering data. The largest effects appeared at backward angles, which is consistent with the naive multiple scattering picture. In contrast to calculations for P_N , here the two-photon exchange effects decrease with increasing beam energy. The $\Delta(1232)$, which dominated the inelastic contributions to this model, tends to cancel the elastic contribution leaving a net effect which is quite small, less than 0.5% at 1000 MeV and $\theta_{CM} = 90^\circ$.

A large number of experiments have measured R^\pm for the elastic channel and found it to be $\simeq 1$ over a large range of beam energy and momentum transfer.[9] The experimental errors were in all cases $>1\%$. The reference of Mar *et al.*[28] summarizes the results of many experiments in a plot versus Q^2 . In Figure 2 we

³By “delicate” we mean that the cross section differences are only a few percent over a large range of $\Delta\epsilon$. In this case, the neglected angular dependence of higher order effects can be relatively large.

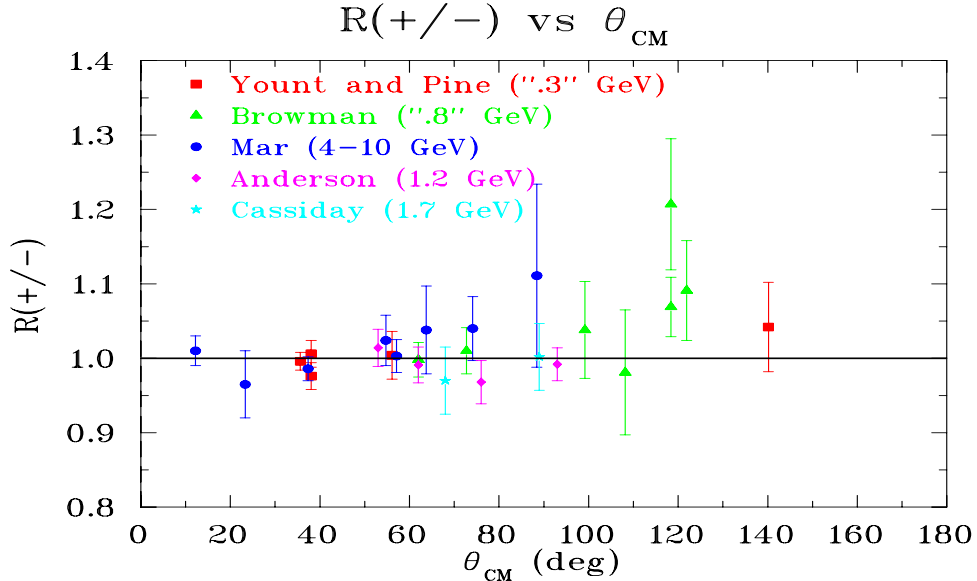


Figure 2: Selection of the world data on the ratio of elastic positron + proton scattering to electron + proton scattering.

have plotted a selection of the world results versus θ_{CM} which is perhaps better motivated. Although this figure shows that a significant two-photon exchange effect has never been convincingly demonstrated in R^\pm , Greenhut's calculations suggest that a low energy, backward angle measurement could succeed if an appropriate facility existed.⁴ However, electron-positron cross section differences may never have high sensitivity, since the predicted effects can be an order of magnitude smaller than the ordinary differential radiative corrections between e^+p and e^-p scattering.

The apparently small magnitude of R^\pm may hold for inelastic scattering as well. The most precise measurements of R^\pm are actually for *inelastic* $e^\pm + p$ scattering at 13.5 GeV at SLAC. The result, averaged over a large range of Q^2 and ν , was $1.0027 \pm 0.35\%$. [29]

summary

With the notable exception of the electron-positron asymmetries, observables which are sensitive to the $Re(\mathcal{M}_2)$ have large backgrounds from single-photon exchange which limit the sensitivity of experiments. The ordinary radiative corrections may be large, or careful kinematic separations must be made to extract the fraction of the two-photon strength which has a non-Born behaviour, or both. The G_E^p crisis and recent Rosenbluth results suggest that two-photon exchange may be important, but it is not clear how to reconcile this with the apparent linearity of the cross section versus ϵ and the small apparent magnitude of σ_2 measured in R^\pm . Plans are being made to learn more about $Real(\mathcal{M}_2)$ via measurements which lack some of the problems of traditional Rosenbluth separations. [7, 8].

⁴Saclay in the early 1990's?

2.4 Imaginary Part of \mathcal{M}_2

Because it has no one-photon backgrounds, P_N (or A_N^T) has a fairly simple approximate structure when expanded

$$P_N = \frac{2N}{\sigma_1} [A_3^* \text{Im}(A_{1_2} + A_{2_2}) + (A_{1_1} + A_{2_1}) \text{Im}(A_3^*)]$$

so knowledge of the one-photon amplitudes will in principle provide relatively straightforward access to the linear combination of two-photon amplitudes $a * \text{Im}(A_{1_2} + A_{2_2}) + b * \text{Im}(A_3^*)$.

2.4.1 the transverse beam spin asymmetry, A_N^e

Wells *et al.* [10] made the first significant observation of two-photon exchange effects on the proton above pion threshold in their measurement of A_N^e , the azimuthal asymmetry in the elastic scattering of *transversely* polarized electrons on unpolarized protons at 200 MeV. Using the SAMPLE apparatus, they found $A_N^e = -15.4 \pm 5.4$ ppm for $\theta_{CM} = 145^\circ$. The observable A_N^e is proportional to the imaginary part of the two-photon exchange amplitude. However, the fact that it requires an electron helicity flip makes it a very different beast from P_N and A_N^T , both from an experimental point of view and from an interpretational point of view. Experimentally, it is suppressed by m/E due to Lorentz suppression of transverse polarization effects. Because of this, the natural scale of the asymmetry is of order $\alpha(m/E) \rightarrow$ few ppm at 1 GeV. Interpretationally, the electron helicity-flip amplitudes correspond to the exchange of quantum numbers which are different than those for other parity-conserving electron scattering observables.

All other things being equal, one would naively expect measurements at higher beam energies to be increasingly difficult due to the m/E suppression of the asymmetry. However, unpublished data from Mainz at 855 MeV show, with very high significance, even larger asymmetries than SAMPLE. This suggests the important role played by inelastic intermediate states at the higher energies. Additional measurements are also being contemplated for JLab.[26]

2.4.2 the normal polarization, P_N or A_N^T

Guerin and Piketty [41] calculated P_N in a model which included only the inelastic contributions from the $\Delta(1232)$ and an additional $\frac{3}{2}^-$ resonance. The energy dependence was fairly complex, first increasing to a maximum of about -0.3% at 560 MeV beam energy, then decreasing in absolute magnitude below 0.1% by 1400 MeV. They separately calculated the contribution from intermediate electron-proton states and found it to be less than half that of the inelastic contribution at all energies.⁵ Although the inelastic model used was simplistic, many important features were demonstrated: threshold behaviour as W exceeds individual resonance poles, the destructive interference of different resonances, and the importance of the inelastic

⁵Numbers were cited for the electron-proton intermediate state but no details or figures were provided.

transition form factors in determining the overall magnitude. It was also clear from this paper that the inclusion of additional resonances could be expected to produce a smoother energy and angle dependence. Compared to the previous estimates by Drell and collaborators[25] of cross section effects, much better dynamical models of two-photon exchange had begun to emerge.

Arafune and Shimizu [42] calculated the contribution to P_N purely from intermediate elastic proton states. The sign of the elastic P_N contribution was found to be opposite to that of the isobar calculation of Guerin and Piketty, suggesting there would be significant destructive interference in a full calculation. Near 1 GeV, the intermediate electron-proton contribution is only about 0.1% and increasing monotonically with energy. Although the calculations predict effects as large as 0.5% at 5-10 GeV, an important kinematic factor was neglected which should be important at higher energies.

Guenter and Rodenberg[43] developed a formalism for both intermediate proton and isobar states, but presented results using only the intermediate proton and $\Delta(1232)$ states. It is nevertheless in some sense the first “complete” calculation, containing the dominant elastic and inelastic contributions. The energy dependence was qualitatively similar to, though often twice the magnitude, of the purely elastic calculations of Guerin *et al.* The calculation reached a maximum of about -0.5% near 550 MeV. By 1 GeV, the calculation develops an oscillating behaviour with a zero crossing near 80 degrees. This behaviour at high energy should not be taken seriously since only intermediate N and Δ states were considered.

A contemporary calculation by Afanasev[5] is shown for 1 GeV beam energy in Figure 3. The model-dependent inelastic contribution is predicted to be several times larger than the model-independent elastic contribution over the standard JLab energy range. Furthermore, P_N is predicted to be a slowly increasing function of beam energy as shown in Figure 4. At forward angles, the calculations are dominated by inelastic contributions. This means that, by varying θ_{CM} from 45° to 90° , the importance of the inelastic contributions in this model ranges from dominant to merely important. Surprisingly, although P_N is predicted to slowly increase with beam energy, the inelastic contributions become relatively *less* important.

The Afanasev calculation uses a model ansatz for the inelastic contribution to the non-forward Compton amplitude with two space-like photons.[30] This model possesses the right crossing symmetry, the correct $Q^2 \rightarrow 0$ limit, and an overall Q^2 dependence which is well-motivated in the GPD limit. Because of the inclusion of a form factor for the inelastic amplitudes, this model does not predict pathologically large upper bounds for P_N as seen in the work of De Rujula[24]. However, only data can establish whether the inelastic contributions have been well-estimated. Some feeling for the large model dependence, at least in the resonance region, can be gained from Figure 14 where calculations from Afanasev, Guenter[43], and Vanderhaeghen[63] are compared. Clearly, $\pm 50\%$ would be a conservative estimate of the model dependence. In the $N + \Delta$ calculation of Vanderhaeghen, destructive interference near 0.570 GeV beam energy causes P_N to nearly vanish, and it remains

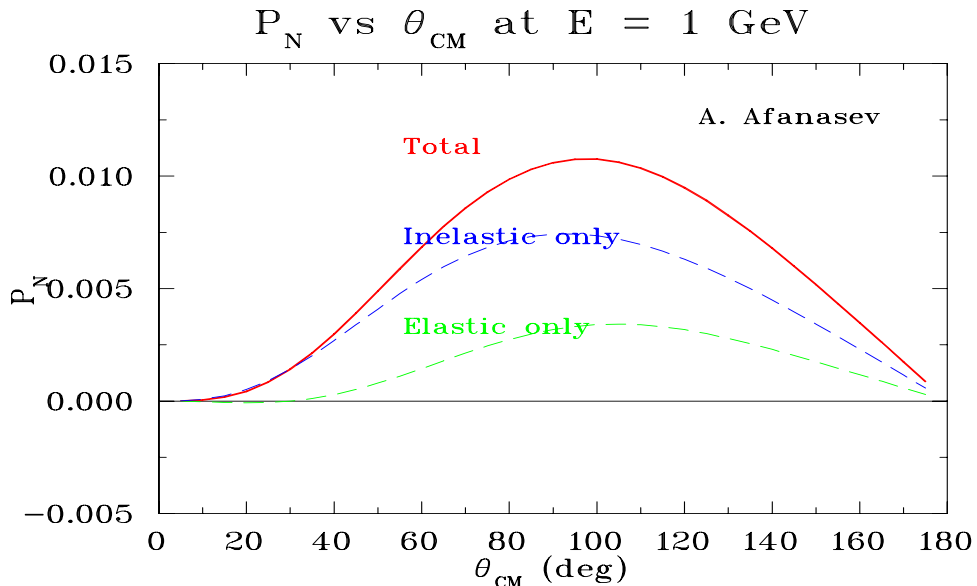


Figure 3: Calculation of P_N for 1 GeV beam energy by Afanasev. ($E_{CM} = 1.66$ GeV) Contributions from the elastic and inelastic intermediate states are shown. Note that the model-dependent inelastic contributions are significantly larger.

small at 0.855 GeV. This degree of cancellation is not seen in either the Guenter or Afanasev predictions.

There are three published measurements of P_N , all with beam energies near 900 MeV and θ_{CM} near 90 degrees.⁶ All lacked the statistical or systematic sensitivity to observe a significantly non-zero result. Bizot *et al.* [31] in their Orsay experiment obtained a result of $P_N = 0.040 \pm 0.027$ which, since it was only 1.5σ , was clearly not a significant observation of two-photon exchange. Systematic errors were treated carefully since there was no means of distinguishing between instrumental asymmetries and a physics asymmetry. Di Giorgio *et al.*[32] made a much less sensitive measurement in similar kinematics at the Frascati electron-synchrotron. Finally, Lundquist *et al.*[33] measured the normal polarization of elastic recoil protons at the Stanford Mark III linear accelerator. They found a null result of $1.3 \pm 2\%$. These three data-sets are compared to a calculation by Afanasev in Figure 5. It is clear that an order of magnitude reduction in error bars will be needed to improve constrain theory.

The $e + d$ elastic scattering experiment of Prepost *et al.*[34] at SLAC probably lacked the sensitivity for a serious search for two-photon effects and is mentioned here only to clarify the historical relationship between P_N measurements and search for violation of time reversal invariance. The vector deuteron polarization at $q = 0.721$ GeV/c was measured to be 0.075 ± 0.088 and was consistent with no effect. Their

⁶We have flipped the sign of those measurements which, since they measured $p(e,p)e'$, used a $\vec{P}_e \times \vec{P}_{p'}$ -based convention which is opposite to our $\vec{P}_e \times \vec{P}_{e'}$ convention.

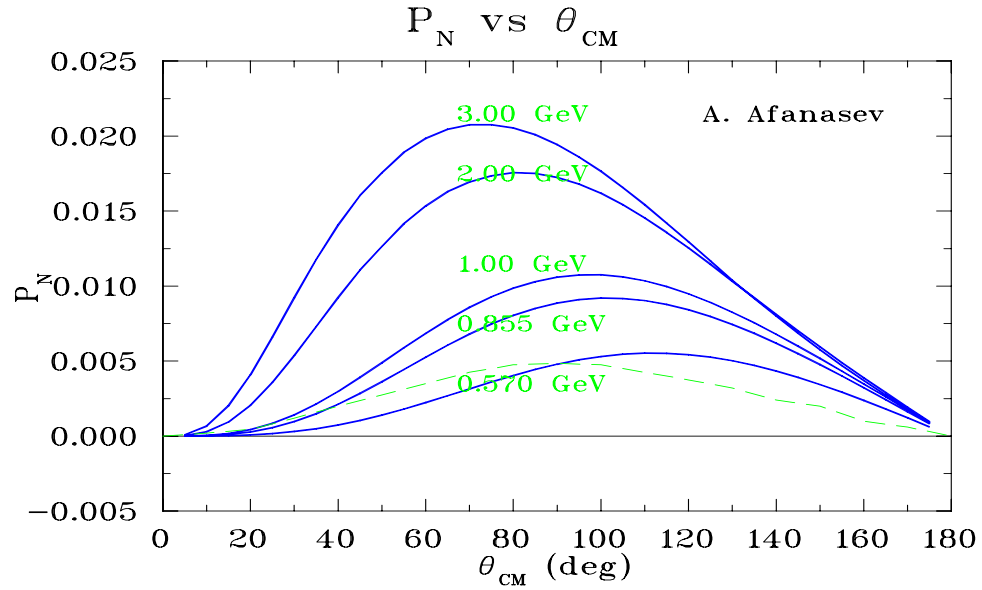


Figure 4: Calculation of P_N from Afanasev for the energies of this experiment. The green dashed line is a calculation from Guenter and Rodenberg [43] at 550 MeV.

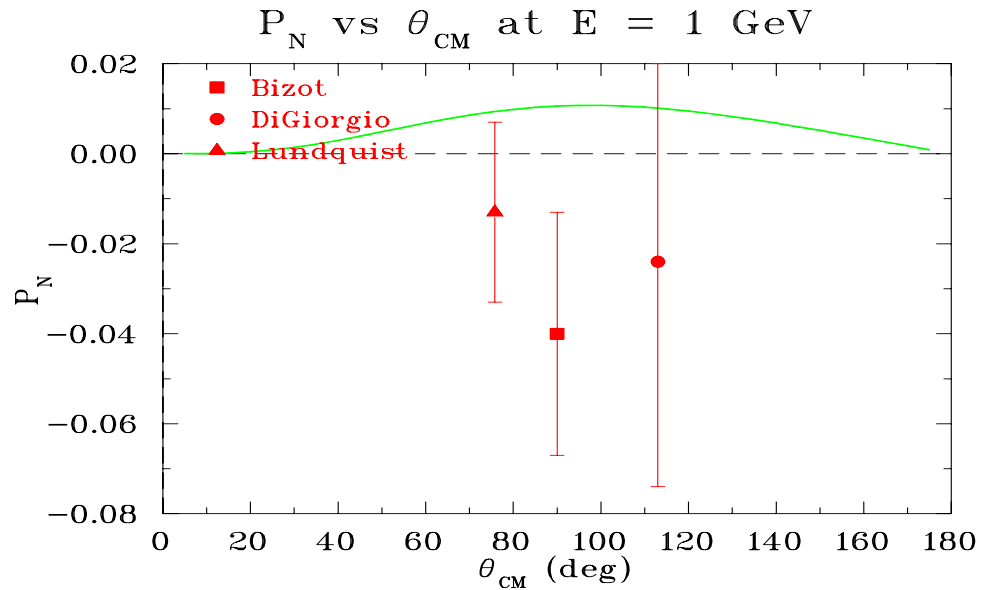


Figure 5: P_N data near 900 MeV versus predictions of Afanasev.

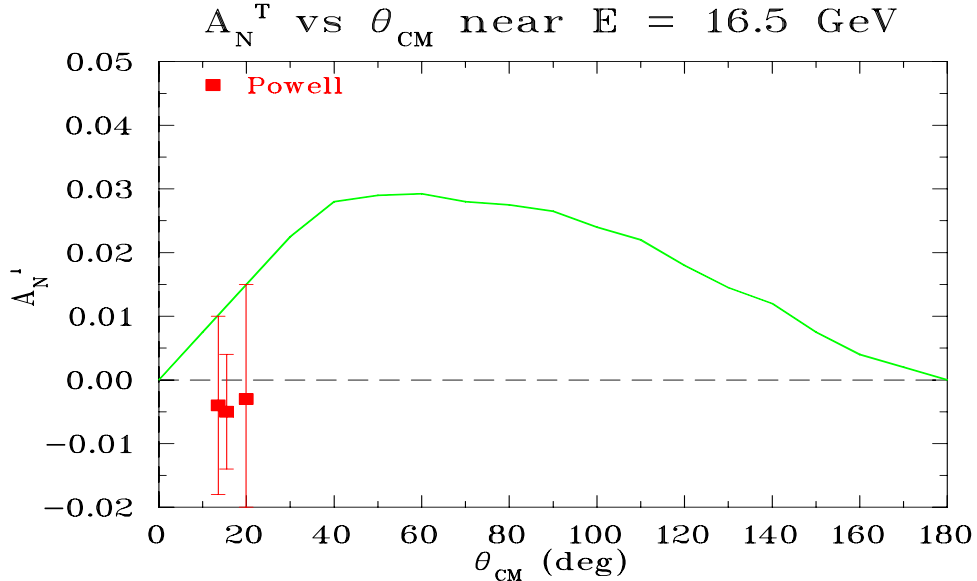


Figure 6: SLAC A_N^T data near 16.5 GeV versus predictions of Afanasev.

measurement was designed to search for a maximal violation of time reversal invariance in the electromagnetic interactions of hadrons which had been hypothesised by Bernstein *et al.*[35] as a possible origin of CP violation, via loops, in the neutral kaon sector.⁷ Following the suggestion by Christ and Lee[36] of several experimental tests, large T-odd contributions to the electromagnetic current were excluded both by Prepost's elastic experiment and Rock *et al.*'s inelastic measurement.[37] Since two-photon exchange effects produce a trivial Standard Model background of order α in P_N measurements, modern experiments instead focus on electric dipole moment (EDM) searches[38, 39] which are zero in the absence of CP odd interactions, have very small Standard Model backgrounds, and are directly related to violation of time reversal invariance under the common assumption that CPT is a good symmetry.

Powell *et al.* [40] at SLAC measured the asymmetry A_N in elastic scattering of electrons from a proton target polarized normal to the electron scattering plane. Because of T-invariance in the electromagnetic interaction, the recoil polarization P_N is equal to A_N . For beam energies of 15 GeV and 18 GeV, θ_{CM} of 13.5° to 20° were explored. Reversal of the target spin direction every 3 minutes was believed to have kept the systematic errors (arising from instrumental drifts) negligible compared to the statistical errors. They found a null result with uncertainties of 1%-2%. Their results, at an average energy of 16.5 GeV, are compared to a 12 GeV prediction of Afanasev *et al.*[30] in Figure 6. (The energy dependence is small compared to the errors.)

summary

⁷Unlike the spin 1/2 proton case, T-odd effects are not forbidden in elastic scattering from the spin 1 deuteron.

Other than the single point from the Wells measurement of A_N^e , none of these experiments made a definitive observation of two-photon effects. Certainly none of them achieved a level of sensitivity which would permit definitive, 3σ measurements of an expected P_N asymmetry of order $\alpha = 1/137 = 0.0073$. This means that existing data only place crude constraints on A_{12} , A_{22} , and A_{32} .

A measurement of P_N via recoil polarimetry has some advantages over a normal polarized target: a pure Hydrogen target with minimal backgrounds, and a generally higher statistical figure of merit (*luminosity* \times *efficiency*). Provided a focussing magnetic spectrometer is used to detect the electrons, a recoil polarimetry experiment will have turn-key isolation of elastic $e + p$ scattering. Focal plane polarimetry for the protons, however, is troubled by false asymmetries because the physics asymmetry is small and there is no mechanism for reversing the sign to cancel false asymmetries. Alternately moving a polarimeter from scattering angle θ_p to $-\theta_p$ to reverse the sign of the asymmetry is a possibility, but the time required to do this, and changes in alignment, suggest it's not appropriate for 0.1% level errors. (One also needs two identical backward angle electron spectrometers, or to somehow move the electron spectrometer from one side of the beamline to another. There is no practical solution.) In order to employ the recoil polarimetry technique for small asymmetries while controlling errors at the 0.1% level, a new technique must be applied to cancel instrumental asymmetries while controlling drifts. This is discussed in the next section.

3 The Experiment

The proton normal polarization, P_N , is small (of order 1% or less), independent of beam helicity, and therefore indistinguishable from a small $\sin \phi$ - or $\cos \phi$ -dependent instrumental asymmetry in a standard recoil polarimeter. Despite meticulous efforts to minimize instrumental asymmetries[31], it has never been measured with high significance. A breakthrough technique is needed which allows the disentangling of the physics and instrumental asymmetries, and which moreover allows one to *prove* that the physics asymmetry has been isolated by demonstrating complete control over the phase of the signal.

We believe that breakthrough technique is a variation on a successful method used to measure the polarization of neutrons in experiments at LAMPF and IUCF.[48, 47] In those experiments the unknown neutron transverse polarization was precessed by $\pm 90^\circ$ before entering a neutron recoil polarimeter. The instrumental asymmetries cancelled in the difference thus isolating the physics asymmetry. For protons, the 50% larger anomalous magnetic moment is very helpful. One superconducting solenoid positioned before the analyzing target will precess the transverse polarization components of the scattered protons up to $\pm 180^\circ$. Thus the effect of P_N in the polarimeter will range from a left-right asymmetry (for 0° or $\pm 180^\circ$ precession) to a top-down asymmetry (for $\pm 90^\circ$ precession). With frequent changes in precession angle, this allows the cancellation of most instrumental asymmetries and long-term drifts. The experimental setup is shown in Figure 7.

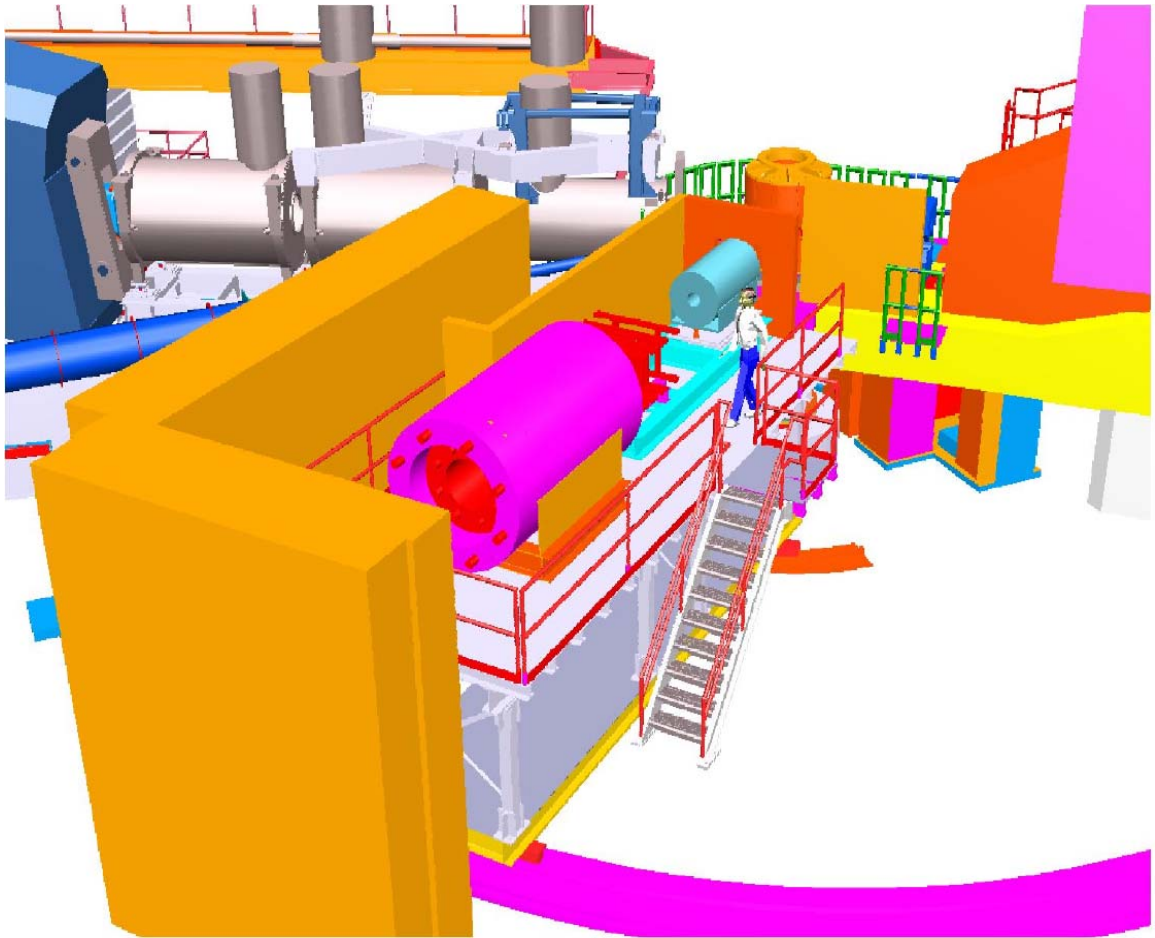


Figure 7: View of the major pieces of hardware in the experiment. Beam enters from the right and exits left. The upright, cylindrical scattering chamber holds LH_2 and LD_2 targets. The HMS is at background left. The hybrid polarimeter is in the foreground, sitting on its carriage which permits rotation from 36.5° to 60° . Electronics racks are located beneath the polarimeter on a sub-floor. The polarimeter is shown without its local shielding for clarity.

3.1 Kinematics

Our choice of kinematics is given in Table 1. It is based on the obvious desire to cover the largest possible range of θ_{CM} subject to time constraints and the limitations of our apparatus. Since the angular dependences are predicted to be quite smooth, this initial survey will cover only two CM angles at each beam energy: approximately 45° and 90° . The choices made regarding E_{CM} coverage are a bit more complicated and discussed next.

By analogy to the dependence on W in photon-nucleon reactions, our expectation is that there will be a complex dependence on E_{CM} in the resonance region, which will simplify for E_{CM} greater than 2 GeV. Measurements at 1, 2, and 3 GeV will allow us to test this assumption, since E_{CM} will vary from 1.66-2.55 GeV. Thus our coverage is from the upper resonance region to well beyond the resonance region. Some of these energies coincide with important JLab electroweak measurements: the $Q_{weak}(proton)$ experiment will run at approximately 1 GeV, and the G^0 , HAPPEX-H and He experiments will run at approximately 3 GeV.

Because two-photon exchange calculations are model-independent below pion threshold, a measurement below about 150 MeV would be an important test of the purely-elastic part of the two-photon amplitude. However, the resulting proton energies are too low for the present apparatus. We suggest this as an interesting possibility for a transverse beam-spin asymmetry measurement.

In the resonance region, the dependence on E_{CM} is potentially very rich. There the highest priority must be a measurement just above the Δ resonance. This will allow a clean test of the model of Vanderhaeghen[63] which includes only the elastic and Δ . Because of the Δ 's strength and the proximity to the nucleon mass, a bare-bones model including only the Δ , in addition to the elastic and the continuum, may already be an excellent approximation to reality. Mainz has completed and is currently analyzing a measurement of the transverse beam-spin asymmetry at 0.570 GeV ($E_{CM} = 1.40$ GeV).[51] By measuring P_N at the same beam energy, complementary information about helicity amplitudes will become available just above the Δ resonance.

The final point in the resonance region we wish to examine is $E = 0.855$ GeV. This corresponds to the existing, but as yet unpublished, data on the transverse beam-spin asymmetry from Mainz. At this beam energy, the center of mass energy, $E_{CM} = 1.58$ GeV, is apparently too high for a model consisting of only the elastic and Δ intermediate channels and underpredicts the data.[52] The complementary information provided by P_N should be helpful.

The solenoidal recoil polarimeter technique can access a wide range of E_{CM} and θ_{CM} to address the following questions:

- Can results above the Δ resonance be understood in terms of a $N + \Delta$ model?, and How important are the higher resonances? These are important questions for developing models of two-photon exchange suitable for the MIT Bates and

Mainz energy ranges, or any future JLab precision electroweak measurements at or below 1 GeV.

- Does the model-dependence simplify above the nucleon resonance region? This is an important question for precision lepton scattering measurements in the multi-GeV regime.

Table 1: Kinematics for the proposed experiment. For P_N , the variables E_{CM} (\sqrt{s}) and θ_{CM} are more appropriate than the traditional choices of Q^2 and θ_{LAB} (or ϵ).

| ID | E_e (GeV) | E_{CM} (GeV) | θ_{CM} (deg) | θ_e (deg) | E'_e (GeV) | Q^2 (GeV/c) ² | θ_p (deg) | T_p (GeV) | Comment |
|----|----------------|-------------------|------------------------|---------------------|-----------------|-------------------------------|---------------------|----------------|-------------------|
| 1a | 0.570 | 1.40 | 102.73 | 80.09 | 0.379 | .36 | 36.5 | 0.191 | "N+ Δ " |
| 1b | | | 56.25 | 39.50 | 0.501 | .13 | 60.0 | 0.069 | or "Mainz Low" |
| 2a | 0.855 | 1.58 | 99.81 | 70.51 | 0.532 | .61 | 36.5 | 0.323 | "Mainz High" |
| 2b | | | 53.81 | 33.61 | 0.742 | .21 | 60.0 | 0.113 | |
| 3a | 1.00 | 1.66 | 98.35 | 66.37 | 0.610 | .73 | 36.5 | 0.390 | "Upper resonance" |
| 3b | | | 52.63 | 31.22 | 0.866 | .25 | 60.0 | 0.134 | or "Qweak" |
| 4a | 2.00 | 2.15 | 89.43 | 46.68 | 1.198 | 1.5 | 36.5 | 0.802 | "Transition" |
| 4b | | | 45.85 | 20.89 | 1.754 | .46 | 60.0 | 0.246 | |
| 5a | 3.00 | 2.55 | 82.40 | 35.69 | 1.874 | 2.1 | 36.5 | 1.126 | "DIS" |
| 5b | | | 41.01 | 15.66 | 2.682 | .60 | 60.0 | 0.318 | or "G0/HAPPEX" |

3.2 Standard Equipment

3.2.1 Electron Spectrometer

The High Momentum Spectrometer (HMS) in Hall C will be used for scattered electron detection. The normal complement of detectors for electron detection consists of drift chambers, scintillator hodoscopes, a Gas Cerenkov, and a Lead-Glass calorimeter. Since the maximum HMS momentum setting will be less than 3 GeV/c, the pressure of the C_4F_{10} in the gas cerenkov can be increased to 0.8 Bar where the mean photoelectron number is approximately 10. The principle purpose for the HMS in this experiment will be to identify elastically scattered electrons by using cuts on invariant mass. It will serve as a clean and stable tag for the presence of elastically scattered protons in the proton polarimeter.

3.2.2 Cryotarget

Standard cryogenic targets of LH_2 and LD_2 in 4 cm diameter tuna-can cells will be employed. The beam will be rastered uniformly by ± 2 mm in x and y on the target in order to minimize density changes. With the tuna-can cell and the new triangular raster pattern, density changes are less than a few percent from 0-100 μA .

3.2.3 Electron Beam Polarimeter

Although P_N is independent of beam polarization, operation with polarized beam allows us to determine P_T which contains valuable information about the product $G_E^p G_M^p / A_Y$. The Basel Moeller polarimeter will be used to measure the beam polarization at least once per beam energy with a reported accuracy of 1%. Variations in beam polarization (due to drifts or current dependence) of up to 3% do not significantly impact these measurements since we have assumed a 5% error on the extraction of $\langle A_Y \rangle$.

3.3 Nucleon Polarimeter

3.3.1 Overview of Nucleon Polarimetry

Nucleon polarizations are measured by scattering from an analyzing target which, through the $L \cdot S$ nuclear force, produces an azimuthal asymmetry proportional to the product of the nucleon polarization and the analyzing power. For example, for a proton polarized vertically, a left-right asymmetry would be produced. The technique is effective at intermediate energies for two main reasons: peak analyzing powers can be several times 10%, and scattering probabilities are of order 1% per g/cm^2 .

As we will see, the polarimeter schematic in Figure 8 has the basic features needed for both proton and neutron polarimetry.

proton polarimetry

For protons, tracking detectors before and after the analysis target establish the scattering angle with high resolution and essentially 100% efficiency. Solid Carbon slabs have historically been the most important analyzing target. At intermediate energies, the largest effective contribution to the analyzing power comes from (quasi-)free $p + p$ and $p + n$ scattering to angles of several 10's of degrees. While there is generally good proton identification before the analyzing target, there is normally only limited proton identification afterwards. Thus, all reactions of the type



are detected, including some which significantly dilute the analyzing power.

The azimuthal asymmetry for a given scattering angle ϕ can be calculated for the normalized distribution $N(\phi)/N_0$ where N_0 is the tracked number of protons

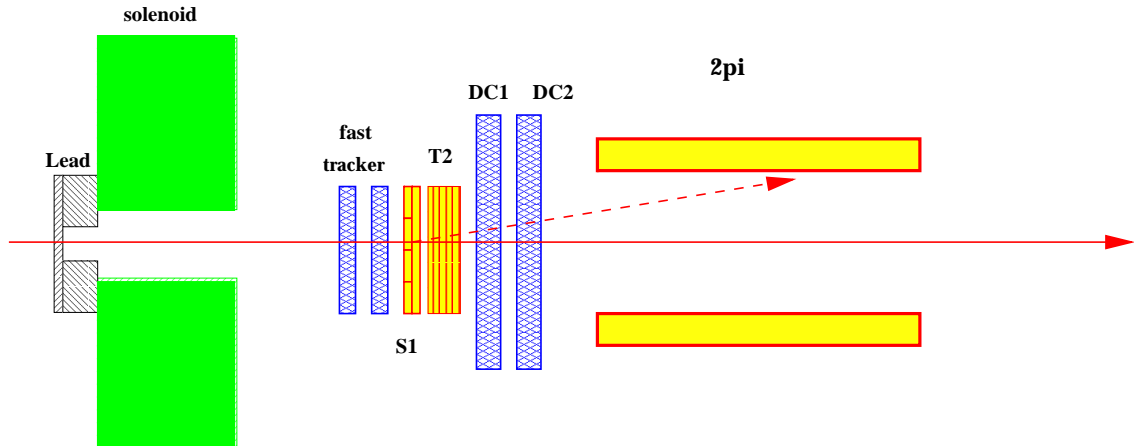


Figure 8: Schematic of the polarimeter. The hatched rectangles represent tracking detectors. S1 is a scintillating trigger hodoscope, T2 is the CH_2 analyzing target (polyethylene), and 2π is a rear cylindrical barrel of scintillator.

incident upon the analyzing target and $N(\phi)$ the scattered distribution seen by the tracking detectors. The analyzing target thickness must not be so large that the tail from Coulomb multiple scattering (which has zero analyzing power) dilutes the larger scattering angle bins which have the largest figure of merit. If this multiple scattering constraint is respected, it is an empirical fact that the figure of merit can continue to increase for thicknesses up to 50 cm in spite of the increasing probability for multiple nuclear reactions in the analyzing target.[49]

An approved JLab proposal for Hall C will employ CH_2 (polyethylene) for its analyzing target because of the higher effective analyzing power.[50] We will also use CH_2 , but with thinner analyzing targets in order to control Coulomb multiple scattering at our generally low Q^2 . By substituting passive CH_2 analyzers for mineral-oil scintillator, one can do neutron polarimetry as discussed in Appendix A.

hybrid vigor

The highest priority of this proposal is make measurements of P_N on the proton in Hydrogen. However, we have investigated significant effort in understanding how to make successful exploratory neutron measurements on Deuterium as well. The design of such a hybrid polarimeter has caused us to realize there are important opportunities for cross-fertilization between what have been traditionally separate technical disciplines.

While our plans for proton polarimetry are robust and traditional, the presence of the rear 2π detector may have some advantages. It seems likely that it will be possible to improve the figure of merit by applying cuts to reject events with excessive inelasticity (and low analyzing power) as is routinely done in neutron polarimetry. Cuts on energy deposited in the active target are much less likely to be beneficial for proton polarimetry, due to the overwhelming energy deposited by the incoming

and outgoing protons via (p, pp) and (p, pn) reactions. However, this will be easy to test.

Neutron polarimetry will benefit from the availability of tracking for charged particles. This will greatly simplify energy and timing calibrations for the front and rear detectors which otherwise have to be done with (predominantly vertical) cosmic rays. For kinematics with higher energy recoil protons, tracking would also make it easier to keep track of (n, n) versus (n, p) -type events. Thus, tracking would reduce the probability that an energetic recoil proton would self-veto an otherwise good neutron scattering event.

3.3.2 Hardware

A thin Lead window will always be in place to shield the detectors from soft electromagnetic backgrounds. In high Q^2 kinematics, where S/N is low but proton energies are relatively high, more Lead can be used so that the experiment can run at higher luminosity. The polarimeter front end is designed to handle 10 MHz of ionizing particles with only a few percent deadtime, and the beam current will be adjusted to achieve this in the polarimeter's small (5 msr) acceptance. A trigger hodoscope (S1) will be used to generate the polarimeter timing reference. A front-end tracking detectors will observe the trajectory of particles entering the adjustable-thickness CH_2 analyzing target, $T2$. (For the lowest proton energies, the trigger hodoscope will be the sole analyzing target.) In some kinematics a thick prototype active target for neutrons may be substituted. The rear 2π detector will trigger when a particle has significantly scattered. A rear tracking detector will provide the most precise measurement of the scattering angle, but is only one of several methods of binning the data in $\Delta\phi, \Delta\theta$.

shielding/carriage infrastructure

As suggested by Figure 7, we plan to construct a new carriage which will allow us to change the polarimeter angle in hours rather than weeks. The carriage will ride on the existing SOS rails and new rails located closer to the pivot. To keep carriage costs under control, the pointing reproducibility will be a modest ± 5 mrad, the weight of detector plus local shielding will be limited to 50 tons, and angle motion will not be motorized. Finer adjustments of solenoid pointing (not the entire carriage) will be done with small motorized screw jacks. The polarimeter angle range for this experiment will initially be $36.5^\circ - 60^\circ$. Electronics will be housed in standard 19" racks on a lower floor of the carriage. With suitable allowance in the design for height variations, the proposed carriage could become a general purpose Hall C facility for the use of other 3rd arm detectors such as Big Cal/BETA.

The two principle sources of background in the Hall are the primary target and the downstream beamline. Detectors will be shielded from the downstream beamline by a stationary wall, and from unintentional direct view of the target by the solenoid's massive iron field clamps. Tight shielding configurations around the detectors will make optimal use of the 50 ton weight budget. There will be no rooms



Figure 9: The Los Alamos/IUCF spin-precession solenoids assumed for the reference design of this proposal. (Photo courtesy of Tom Rinckel (IUCF))

large enough for humans to walk around in, but doors will allow access to work on detectors.

solenoid

To rotate the proton spin a full $\pm 180^\circ$ for our proposed kinematics, the superconducting solenoid requires a total field integral of approximately 5 Tesla-meters. The free bore should be large enough to accommodate most of the elastic proton beam envelope conjugate to the HMS elastic electron acceptance. An available pair of solenoids have been located at IUCF which appear to satisfy these requirements. We plan to use only one of them and hold the other in reserve. Solenoids nts0 and nts1 were originally built for LAMPF, then later transferred to IUCF to become part of the INPol (Indiana University Neutron Polarimeter) Facility.⁸ Although IUCF remains an active facility for material science, radiation effects, and medical physics, the nuclear physics operations have been shut down and the solenoids are no longer needed there.

The solenoids are presently contained in 1" thick iron casings which serve to return flux and reduce stray fields while retaining azimuthal symmetry. However, TOSCA simulations indicate that, at large excitations, the present iron casing will saturate near the bore opening leading to large stray fields[53]. Additional iron was added to each end in the TOSCA simulation, corresponding to the geometry in Figure 10. This reduces the field to about 5 Gauss roughly 0.5 meter from the opening, and to about 1 Gauss at 1.5 meters from the opening as shown in Figure 11. The nearest detectors will be approximately 1.5 meters from the opening.

⁸The cryostats were built by Janis and the coils by American Magnetics, Inc.

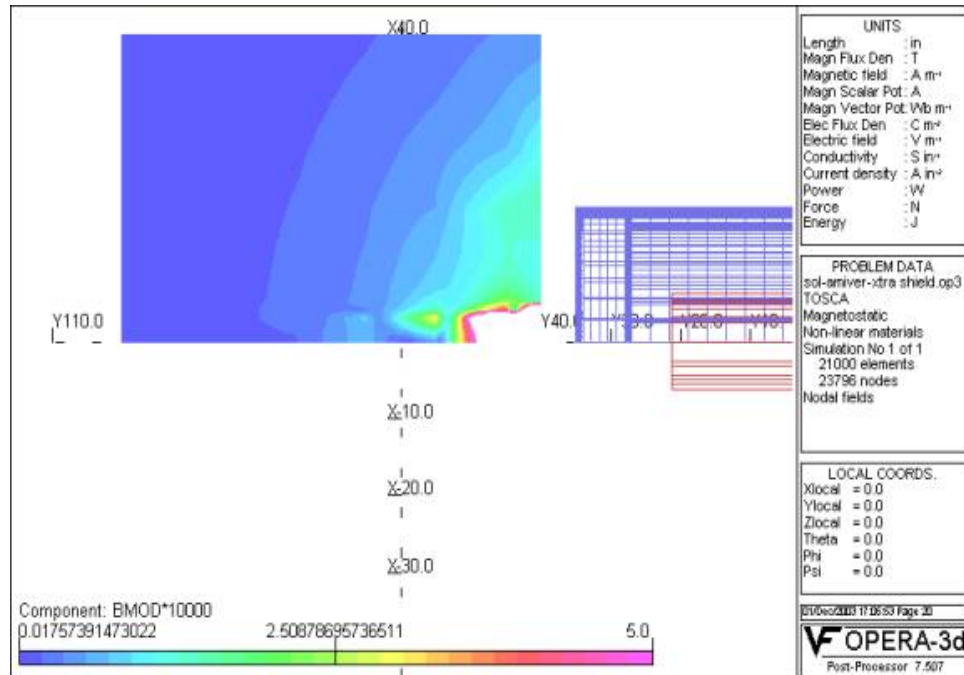


Figure 11: TOSCA simulation of the external fields. The vertical X-axis corresponds to the solenoid radial coordinate to a maximum of 40 inches, while the horizontal Y-axis is the longitudinal coordinate to a maximum of 110 inches (2.8 meters). The color bar is a linear representation of the field strength, from 0 Gauss to 5 Gauss. In the lower right hand corner of the colored rectangle, the first color is the 5 Gauss contour. The first detectors would begin at 1.5 meters in a 1 Gauss field.

Table 2: Specifications for the LANL/IUCF solenoids nts0 and nts1.

| Property | Value |
|--------------------------|--|
| Length | 1.47 meters |
| Diameter | 0.78 meters |
| Free Bore | 0.20 meters |
| Nominal I _{max} | 300 Amps |
| Field Integral | I*0.164/10 Tesla-meters (IUCF map of nts0) 4.92 Tesla-meters (at I _{max}) |
| Central Field | I*0.01383 Tesla 4.15 Tesla (at I _{max}) |
| Effective Length | 1.19 meters |
| ramp rate | 300 A in 6 minutes (0.83A/min) |

meets our specifications, a duplicate chamber, offset by 20 cm along the polarimeter beamline, would improve angle resolution and tracking efficiency.

trigger hodoscope (S1)

The front-end trigger detector must have approximately 100% efficiency for rates up to 10 MHz. It must be $\simeq 1$ cm of CH_2 equivalent thickness because it will serve as the analyzing target for 70 MeV protons in our lowest Q^2 configuration. The meantime resolution must be < 300 psec to be consistent with single beam burst coincidence timing with the HMS.

These specifications can be met by a scintillating hodoscope consisting of 2 planes in a U-V configuration. The active area would be 30 cm x 30 cm, with 10 non-overlapping strips per plane. Each strip would be 0.50 cm thick. With 1" pmt's and clipped anode signals, the resulting 10 nsec wide pulses will result in a deadtime per channel of only 1%. Fewer than 1% of events will have 3 or more tracks. (The familiar 4-fold ambiguity in the 2-hit events is easily resolved using the front-end wire chamber information.) Each element will have a short lightguide and a pmt on each end, for a total of 40 pmt's.

CH_2 analyzing targets

Depending on proton kinetic energy, the thickness of the CH_2 analyzing targets will be adjusted to keep the rms Coulomb multiple scattering angle approximately 0.9° , up to a maximum target thickness of 40 cm. Coulomb multiple scattering has zero analyzing power, and if not controlled could dilute the figure of merit of otherwise useful nuclear scatterings to small angles. The planned thicknesses for proton running for all kinematic settings can be found in Table 5 at the end of this proposal. We plan to use all protons which scatter to angles larger than roughly 3° .

prototype active target

Because the prototype active target is required only for exploratory neutron measurements it is discussed in the Appendix A.

rear 2π detector

A rear trigger detector is needed which has essentially 100% efficiency for scattered protons in the angle range 3° to 45° (somewhat adjustable), and mean timing resolution better than 300 psec. It should be insensitive to the very high rate of straight-through particles and to ± 1 Gauss changes in magnetic field. The rear trigger detector must provide a means of binning scattered protons into $\Delta\phi, \Delta\theta$ which is completely independent of wire chamber information.

These specifications can be met by a long cylindrical barrel of scintillator, constructed from 16 long slightly overlapping "staves" of scintillator with a pmt on each end. The straight-through particles will pass down the barrel axis undetected. Because of its complete azimuthal acceptance, it is called the 2π detector. The 2π hit location is obtained from the bar number and the calibrated difference of the TDC's on each end. (Double-hits in overlapping counters will be sorted randomly to one bar or the other.) Combined with front-end tracking information, this can be

used to bin the data in $\Delta\phi, \Delta\theta$. In an analysis without front tracking chambers, the HMS will be used to predict the proton angle, and the χ -dependent false asymmetry due to solenoid steering must be measured with X-Y modulating coils and corrected. The barrel can be shifted slightly up or downstream to adjust the minimum scattering angle. Because the barrel will be nearly 300 cm long, a thickness of 2.5 cm will ensure the mean time resolution meets specification.

rear tracking

The rear tracking detectors are used in only one of the three analysis methods for this experiment. They would provide a means of binning scattered protons in $\Delta\phi, \Delta\theta$ while using the 2π detector only as a trigger for scattered protons. We could do the experiment without it, using two other analysis methods, but the rear chamber would provide a valuable cross check and would be useful for calibrating the 2π detector. The scattering angle coverage required for protons is 1° to 45° (measured from the center of the CH_2 target rack), with full azimuthal acceptance. To minimize the potential for biases, we suspect the tracking efficiency must be $>98\%$ with a total ionizing particle rate of 10 MHz. The rescattered proton angles must be determined with < 5 mrad angle resolution, and the reconstruction must be perturbed less than 0.5 mrad by ± 1 Gauss changes in the ambient magnetic field.

The working concept for a detector that meets this specification is to use a *pair* of horizontal drift chamber with an active area of 100 cm x 100 cm, six wire planes in a X-Y-U-V-X'-Y' configuration, and 0.5 cm sense wire spacing (half that of the current HMS wire chambers). With an average drift time of about 40 nsec, the deadtime per wire will be less than 1% and only about 5% of events will have 3 or more tracks. While a single chamber is sufficient to meet the angular resolution specification, the adjacent second chamber (offset by 1/2 cell spacing) would provide the redundancy needed to meet the efficiency specification.

More detailed study is needed to understand the relationship between the efficiency specification and potential sensitivity to χ -dependent false asymmetries. Multiple chambers will help increase efficiency in the presence of noise, but the efficiency may ultimately be limited by the ability to resolve 3 tracks in the hot straight-through region of the chamber. In the worst case scenario, we would drop this analysis method but still employ a simple rear chamber to help calibrate the 2π detector.

3.3.3 Alignment

Before the experiment, the solenoid must be fiducialized, field-mapped at several excitations, and have the mechanical and magnetic center lines determined. In parallel, a lot of experience with the control system, ramp rates, LHe consumption rates, stray magnetic fields, and alignment tolerances will be obtained.

The solenoid table will be mounted on a larger arm which holds (in increasing order from the target): “soft” EM background shielding, a collimator ladder, the solenoid table, front tracking detectors, a scintillating trigger hodoscope (S1), a

rack for CH_2 slabs (T2), rear tracking detectors, and the 2π detector. Except for the shielding, these items will be aligned with the magnetic axis to help minimize instrumental asymmetries. The polarimeter will basically consist of three modular units (solenoid, main detector package, and 2π section) which can be assembled outside the Hall, trucked in, craned into place, and finally aligned.

During the experiment, for each new kinematic setting, alignment begins by moving the electron arm and recoil polarimeter to their nominal angles for elastic $e + p$ coincidences. We assume that a rail system exists which will quickly allow the solenoid axis to be aligned with the central proton ray within ± 5 mrad. This is sufficient for the experiment, but will be checked by the following procedure:

The solenoid fields will be *off* for initial alignment check. A collimator with a single small central hole (“pin-hole”) along the magnetic axis will be inserted in front of the solenoids. At the exit of the solenoids, the front-end tracking detectors will view the transmitted elastic proton beam spot. Small adjustments to the polarimeter scattering angle and the vertical position of the beam spot on the cryotarget will align the proton beam within a few mrad of parallel with the known magnetic axis. At this point, turning on the solenoid to maximum field should move the proton spot only slightly. Further adjustments of the polarimeter pitch and yaw can be made with the solenoid at maximum field to finalize the alignment.

3.3.4 Absolute Determination of P_N

The absolute determination of P_N from the experimental physics asymmetry depends on the value of the secondary target analyzing power, A_Y , as

$$P_N = \langle A_N^{exp} \rangle / \langle A_Y \rangle \quad (17)$$

To some extent, we can use published values from similar polarimeters if we wish to use Carbon as the analyzer. However, since the beam will be polarized, we can use the large, helicity-dependent asymmetry A_T^{exp} . This is discussed in the section on systematic errors.

3.4 False Asymmetries and Spin Precession

We define *intrinsic* false asymmetries to be those which are not directly produced by the act of precession (*e.g.* a detector which is inefficient in one region), and *induced* false asymmetries to be those created by act of precession (*e.g.* steering of the protons by a misaligned solenoid). The separation of the false asymmetries into intrinsic and induced versions is artificial but helps in understanding the issues.

For an ideal beam of protons parallel to the solenoid axis, the only important false asymmetries for a recoil polarimeter with proper magnetic shielding are intrinsic ones. Even a well-constructed and well-aligned polarimeter may have false asymmetries $\simeq 0.5\%$ due to residual mis-alignments, imperfect dead-time corrections and other unaccounted-for variations in detection efficiency. For a significant measurement of P_N , these false asymmetries must be removed since they are of the same order of magnitude as the anticipated signal.

Precessing the spin of the protons is the key to cancelling the intrinsic asymmetries. Without precession, P_N will produce a small left-right asymmetry in the polarimeter which is virtually indistinguishable from an instrumental asymmetry. Neutron polarimeters at LANL and IUCF[48, 47] have successfully used solenoids to precess the transverse spin components $\pm 90^\circ$ to cancel instrumental asymmetries. However, in our setup more care must be taken to avoid inducing significant false asymmetries. First, because protons are charged they receive small deflections from finite alignment tolerances, and angular divergence of the proton beam causes the envelope to rotate. Second, one has to minimize the effects of stray magnetic fields on the primary beamline and the polarimeter detectors.

We will minimize and deal with potential false asymmetries by:

- iron encapsulation of the superconducting solenoid to reduce the stray fields
- tracking the proton into and out of the analyzing target to properly bin events in rescattering angle, in spite of $O(5\text{mrad})$ shifts in the angle of the proton beam,
- in a separate analysis in which no chambers are used on the proton side, the false asymmetries will be measured with 30 Hz X-Y modulation of the proton beam envelope,
- varying the precession in 90° steps to $\pm 180^\circ$, isolating P_N by the $\cos(\phi + \chi)$ dependence

3.4.1 basic spin precession facts

The proton precession frequency is calculated as

$$\omega = \frac{geB}{M_p} = g(9.579 \cdot 10^7)B \text{ radians/second} \quad (18)$$

with B in units of Tesla, M_p is the proton mass, and using $\mu_p = 2.7928$. The angle χ through which the proton spin vector precesses is therefore

$$\chi = \omega \frac{\Delta t}{\gamma} = \omega \frac{L}{\beta c \gamma} = 51.1^\circ \frac{M_p}{P} \int BdL \quad (19)$$

where P is the proton momentum. The field integral required to precess the spin by an angle $\theta = 90^\circ$ is

$$\int BdL = 1.76P/M \quad (20)$$

Field integrals of .56-3.2 Tesla-meters are needed to precess protons of 100-1000 MeV kinetic energy by 90° . For neutrons of the same P/M , field integrals 1.46 times larger⁹ are required due to the smaller g-factor. In Table 3 are listed the field

⁹ $\mu_p/\mu_n = 2.7928/1.9130 = 1.46$

integrals required for the all the kinematic settings in the experiment. Protons will be precessed up to 180° in order to map out the $\cos(\phi+\chi)$ dependence of the physics asymmetry. In a few settings, we cannot reach the full $\pm 180^\circ$ precession due to the 5 Tesla-meter limitation of the single solenoid we plan to use for Phase I.

Table 3: Field integrals required at the planned kinematics to precess protons or neutrons by $\pm 90^\circ$, $\pm 180^\circ$.

| ID | E_e (GeV) | E_{CM} (GeV) | θ_{CM} (deg) | proton $\int BdL$ 90° | proton $\int BdL$ 180° | neutron $\int BdL$ 90° | neutron $\int BdL$ 90° |
|----|----------------|-------------------|------------------------|---------------------------------|----------------------------------|----------------------------------|----------------------------------|
| 1a | 0.570 | 1.40 | 102.7 | 1.178 | 2.356 | 1.718 | 3.426 |
| 1b | | | 56.3 | 0.690 | 1.380 | 1.006 | 2.012 |
| 2a | 0.855 | 1.58 | 99.8 | 1.581 | 3.162 | 2.306 | 4.612 |
| 2b | | | 53.8 | 0.890 | 1.780 | 1.297 | 2.594 |
| 3a | 1.00 | 1.66 | 98.4 | 1.763 | 3.526 | 2.571 | 5.0 (175°) |
| 3b | | | 52.6 | 0.972 | 1.944 | 1.418 | 2.836 |
| 4a | 2.00 | 2.15 | 89.4 | 2.749 | 5.0 (164°) | 4.014 (skip) | 8.028 (skip) |
| 4b | | | 45.9 | 1.355 | 2.71 | 1.975 | 3.950 |
| 5a | 3.00 | 2.55 | 82.4 | 3.448 | 5.0 (131°) | 5.03 (skip) | 10.06 (skip) |
| 5b | | | 41.0 | 1.568 | 3.136 | 2.286 | |

3.4.2 Intrinsic False Asymmetries

A simple but powerful piece of physics is helpful to our separation of P_N from the experimental asymmetries: *For unpolarized beam, proton polarization components other than P_N are forbidden in the absence of parity violation.*¹⁰ Given our modest Q^2 and limited statistical sensitivity of roughly 300ppm, parity violation can be ignored. This means that for unpolarized beam, P_T and P_L are zero, even when such complications as multi-photon exchange are taken into account. Hence any (beam helicity averaged) statistically significant asymmetry in the P_T direction is the instrumental asymmetry.

Looking along the proton momentum, the coordinates are defined in Figure 12. Because the HMS is located beam right, the direction of a positive P_N is $\vec{P}_e \times \vec{P}'_e$ or toward the floor. For unpolarized or helicity-averaged beam, the azimuthal

¹⁰The only Hamiltonian which can be constructed from the available momentum and non-zero polarization vectors, and yields a non-zero P_L or P_T , is $\vec{\sigma}_p \cdot \vec{p}_p$ which is P-odd and T-even. It can be identified with Z exchange and its magnitude estimated accordingly.

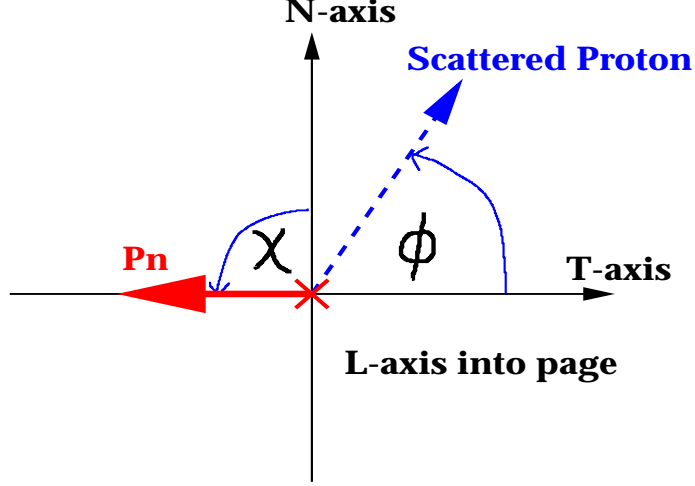


Figure 12: Looking along the proton incident momentum (or L-axis), the precession angle χ and the proton azimuthal scattering angle ϕ are defined. In this example the proton normal polarization has been precessed by $+90^\circ$. Since the HMS is beam right, the \hat{N} axis is actually pointing toward the floor.

asymmetry of scattered events becomes

$$A_{exp}^{\chi}(\phi, \theta) \equiv \frac{N^{\chi}(\phi, \theta)}{N_0^{\chi}} - 1 = A_Y(\theta)P_N \cos(\phi + \chi) + A_N^{false}(\theta) \cos \phi + A_T^{false}(\theta) \sin \phi \quad (21)$$

where N_0^{χ} is the number of protons incident on the analyzing target, θ is the angle of the secondary scattering, ϕ is the azimuthal coordinate of the scattered proton, and χ is the precession angle of the proton spin. Here N_0^{χ} is rigorously interpreted as the absolute number of incident proton events which meet all criteria such as ‘‘HMS elastic electron’’, ‘‘good coincidence time’’, and ‘‘good front-end track’’. Meanwhile, $N^{\chi}(\phi, \theta)$ meets the same good beam criteria (so that charge, target density, and front-end efficiencies cancel) but bins data in $\Delta\phi, \Delta\theta$ using one or more possible detectors. By taking data at two precession angles differing by 180° , the physics asymmetry is isolated by taking the difference of the normalized distributions:

$$A_{exp}^{\chi, \chi+\pi}(\phi, \theta) \equiv \frac{N^{\chi}(\phi, \theta)}{N_0^{\chi}} - \frac{N^{\chi+\pi}(\phi, \theta)}{N_0^{\chi+\pi}} = 2A_Y(\theta)P_N \cos(\phi + \chi) \quad (22)$$

Thus precession of the proton spin by the solenoids causes the phase of the physics signal to vary with $\cos \chi$ while leaving the intrinsic false asymmetries unaffected. For the specific example of $\chi = \pm 90^\circ$, taking the difference, the $\cos \phi$ moments, and appropriate averages over θ :

$$P_N = \frac{-1}{2\pi \langle A_Y \rangle} \int_0^{2\pi} \left[\frac{\langle N^{\chi=+90^\circ}(\phi) \rangle}{N_0^{\chi=+90^\circ}} - \frac{\langle N^{\chi=-90^\circ}(\phi) \rangle}{N_0^{\chi=-90^\circ}} \right] \sin \phi d\phi \quad (23)$$

where the $\langle \rangle$ represent θ -averaged values. The instrumental asymmetries can be determined along the Left-Right axis (which has no physics asymmetry by parity

conservation):

$$A_{LR}^{false}(\theta) = \frac{1}{2\pi} \int_0^{2\pi} \frac{N^{\chi=\pm 90^\circ}(\phi, \theta)}{N_0^{\chi=+90^\circ}} \cos \phi d\phi \quad (24)$$

or by addition along the Top-Bottom axis (to cancel the physics asymmetry):

$$A_{TB}^{false}(\theta) = \frac{1}{2\pi} \int_0^{2\pi} \left[\frac{N^{\chi=+90^\circ}(\phi, \theta)}{N_0^{\chi=+90^\circ}} + \frac{N^{\chi=-90^\circ}(\phi, \theta)}{N_0^{\chi=-90^\circ}} \right] \sin \phi d\phi \quad (25)$$

and studied for long term stability.¹¹ Assuming a dataset consisting of precession angles $\chi = -180^\circ, -90^\circ, 0^\circ, +90^\circ$, and $+180^\circ$, many such equations can be written down, with many possible cross-checks on both the physics and false asymmetries.

In reality, of course, we will do a likelihood analysis based on equation 21. Perhaps the best way to visualize the power of this approach is to project the equation 21 onto A_{LR} and A_{TB} as in Figure 13. For demonstration purposes, the false asymmetries were set to reasonable values of 1% for A_{LR} and -5% for A_{TB} , while the physics asymmetry for $P_N = 1\%$ is $A_{phys} = A_Y P_N = 0.4 * 1\% = .4\%$.

To ensure that we are able to cancel false asymmetries which may vary with time, we will normally vary the precession angle by 180° every 15 minutes. This will cost us approximately 3 minutes of experiment deadtime out of every 15 minutes, or 20% “reversal deadtime”.

3.4.3 Induced False Asymmetries

Small induced false asymmetries are ultimately not fatal to the experiment since the physics asymmetry has a well defined $\cos(\chi + \phi)$ dependence. However, it is a good policy to minimize and measure all false asymmetries which change with precession angle. This is analogous to the measurement of small parity-violating asymmetries in which changes in the beam helicity at the source produce small changes in beam position or angle on the target. After first minimizing the helicity-dependent changes, one can measure and correct the data for any remaining effects.

precession-dependent steering

The fact that protons are charged means that small misalignments between the proton velocity and the solenoidal field can change the position and angle of the proton beam as a function of the solenoidal field. A skew angle θ_{skew} will steer the angle by

$$\Delta\theta_{steer} = 0.3 \frac{\sin \theta_{skew} \int B dl}{P} \quad (26)$$

We derived previously that the field integral required to precess the proton spin by a fixed angle is proportional to the momentum, P , hence

$$\Delta\theta_{steer} = 0.3 \frac{\sin \theta_{skew} 1.76}{M_p} \simeq 0.56 \theta_{skew} \frac{\chi}{90^\circ} \quad (27)$$

¹¹It should not be forgotten that our coordinate system is not frozen in the polarimeter frame but changes slightly event by event referenced to $\vec{P}e \times \vec{P}e'$ and $\vec{P}e - \vec{P}e'$.

Asymmetry vs Precession Angle

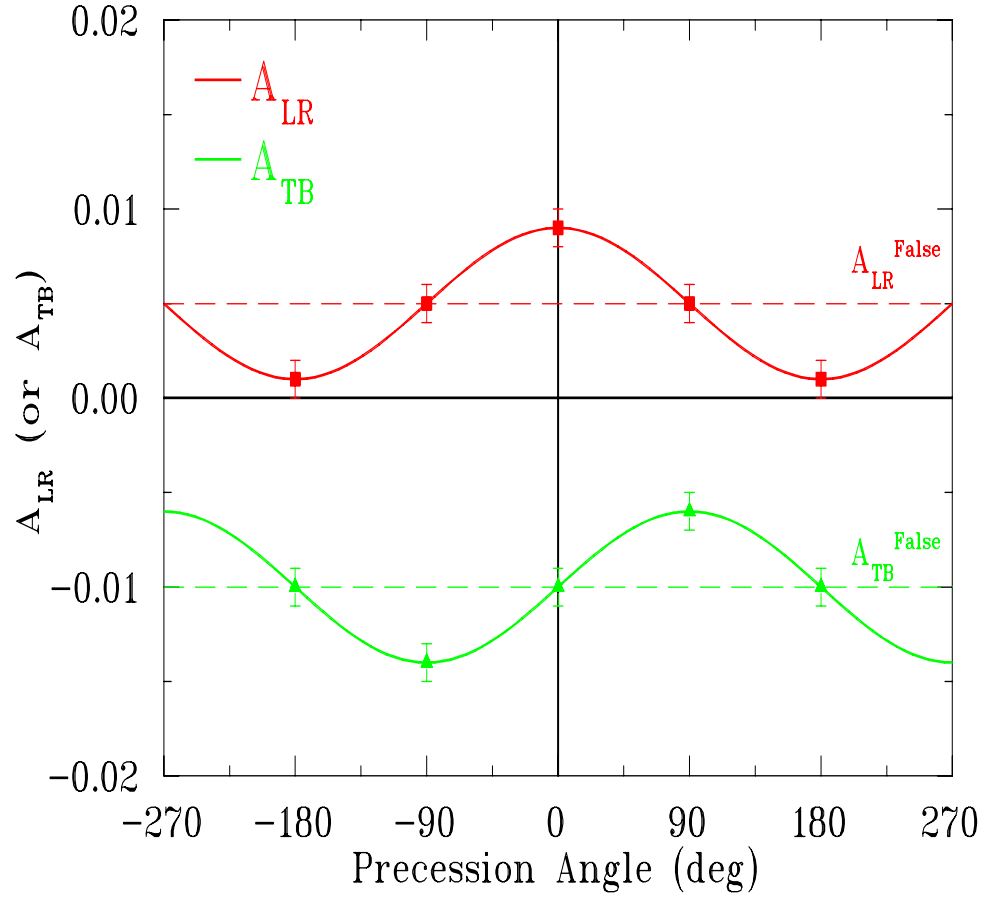


Figure 13: A global way of visualizing the dataset corresponding to a typical E_{CM}, θ_{CM} point in this experiment. For demonstration purposes, the false asymmetries were set to reasonable values of 1% for A_{LR} and -0.5%, and the physics asymmetry is taken to be $A_{phys} = A_Y P_N = 0.4 * 1\% = 0.4\%$. The statistical error per point is 0.1%.

A typical post-alignment “yaw” of 2.5 mrad in the horizontal plane, combined with a precession angle change of $\pm 90^\circ$, would move the beam envelope on the analyzing target up and down by ± 2.5 mm, and vary the incident angle by ± 1.4 mrad. Without tracking detectors to correct for such precession-dependent angle changes, false asymmetries of $O(1\%)$ could result simply due to the angular dependence of the nuclear scattering cross section. Furthermore, without tracking detectors to correct for the small position change, smaller but still significant false asymmetries of $O(0.1\%)$ would result from the resulting changes in solid angle.

These steering effects can be handled by three very different techniques in the same apparatus:

- The first technique is to use front-end tracking and rear tracking to sort rescattered protons into the proper $\Delta\phi, \Delta\theta$ bins.
- The second technique is to use front-end tracking and the 2π detector to bin data in $\Delta\phi, \Delta\theta$, assuming that the scattering took place in the target at the midpoint of the projected front-end track.
- A possible third technique is to not use any tracking detectors in binning, but to use a tight HMS-S1 coincidence to define the incident flux N_0 , use the HMS to predict the proton angle, and use the projected midpoint of the analyzing target and the 2π detector to bin in $\Delta\phi, \Delta\theta$. Without further corrections for steering, this technique would suffer from $O(1\%)$ false asymmetries. However, the false asymmetries could be measured during data-taking with coils that move the beam at 30 Hz over a similar range of position and angle. This is similar to the philosophy of parity violation measurements, although in our case the corrections would be of $O(100\%)$.

We plan to use all three techniques. Even if one of the schemes turns out to be unworkable for technical reasons (or incapable of reaching our 0.1% sensitivity goal), the two other techniques will still provide a cross-check. We emphasize that these are established techniques in the fields of proton and neutron polarimetry and parity violation. The only new aspect is our application of these techniques to the problem of a less-than-perfect, solenoidal proton polarimeter.

precession-dependent detector efficiencies

The effect of stray magnetic fields on detectors is one potential source of induced false asymmetry, one that is not unique to our solenoidal recoil polarimeter technique. We have attempted to strangle this problem by passive shielding which retains the azimuthal symmetry of the polarimeter as discussed in section 3.3.2. The efficacy of these shielding efforts will be verified by mapping the field. Standard shielding techniques for Gauss-level magnetic fields will be used for the detectors: distance as well as iron and μ -metal shields. Any residual effects of stray solenoid fields on pmt’s can be determined, and resolved as needed, in the Test Lab with an LED-based gain monitoring system such as that proposed for the Hall B Primex

experiment.[54] Setting detector thresholds in hardware and software well below typical proton energy deposits will cause minor changes in gain to have negligible effect on efficiency.

Once the polarimeter is aligned, any precession dependent false asymmetries can be adequately described to second order in χ . The azimuthal distribution of events in the polarimeter generalizes to

$$\begin{aligned} \frac{N^\chi(\phi)}{N_0^\chi} &= 1 + A_Y(\theta)P_N \cos(\phi + \chi) \\ &+ (A_{LR}^{false} + A_{LR}^{false'} \chi + A_{LR}^{false''} \chi^2) \cos \phi \\ &+ (A_{TB}^{false} + A_{TB}^{false'} \chi + A_{TB}^{false''} \chi^2) \sin \phi \end{aligned}$$

3.5 Backgrounds

particle identification

The HMS trigger will be set to detect essentially all electrons as well as a sample of π^- events. Electrons will be cleanly identified offline by a combination of cuts on the number of photoelectrons in the Gas Cerenkov and the E_{cal}/p response of the Electromagnetic Calorimeter. We are free to make these offline cuts quite tight since the only downside will be a small loss of efficiency. Pion rejection will therefore be at the 10^{-5} level. Recoil proton kinematics are then predicted by two-body kinematics.

The polarimeter will be able to distinguish between charged and neutral particles using a combination of trigger scintillators and a front-end tracking detector. For events with an elastic electron in the HMS, the time of flight (TOF) to the polarimeter and the angle incident on the analyzing target will provide redundant information about the elastically scattered protons.

Inelastic backgrounds on Hydrogen

Protons arising from inelastic reactions on Hydrogen (*e.g.*, $e + p \rightarrow e + \pi^0 + p$) can have potentially large normal polarizations due to strong interactions. Inelastic contamination at the 1 per 100 level, if uncorrected, would saturate our systematic error budget of 0.1%. No correction is expected to be necessary since inelastic protons will become negligible after cuts on the invariant mass

$$W = \sqrt{-Q^2 + M_p^2 + 2\nu M_p} \quad (28)$$

where $\nu \equiv E_e - E'_e$ and in terms of 4-vectors, $Q^2 \equiv -(e - e')^2$. With a resolution of 10 MeV (rms), there is an enormous separation between the elastic peak and pion threshold. Note that the invariant mass is reconstructed from electron arm information, so it is unaffected by the precession angle in the polarimeter arm.

Coincidence time and proton angle cuts are available to suppress inelastic backgrounds but are completely redundant if the target is pure Hydrogen. However,

these cuts will be useful for suppressing both random coincidences and the tail of the Δ resonance in quasi-elastic $D(e, e'N)N_s$ scattering.

background reactions on nuclei

Approximately 10% of the protons in a 4 cm target are in the windows, and protons from quasi-free $(e, e'p)$ knockout from the Aluminum target windows could easily have P_N^{Al} of 10% at the low recoil momentum corresponding to the $\pm 1^\circ$ acceptance of our polarimeter.[60] Unmitigated, this would produce a physics asymmetry of 1%, or as large as the typical expected signal. In practice, Aluminum window background yields are typically only 1% in $e + p$ elastic scattering after an invariant mass cut. Hence the Aluminum background asymmetry contributes only at the 0.1% level. This is small but at the same level as our sensitivity goal; we will therefore spend 1% of our running time on Aluminum dummy cells which have 10 times the normal window thickness. The time required is so short it does not appear in the beam request.

The same process can occur on trace Deuterium in the LH_2 target, although the low Deuterium concentration (0.1%) and the lower FSI probability make this contribution negligible. In an experiment at MIT Bates, the measured value of P_N on deuterium at $Q^2 = 0.38$ and 0.50 was zero within errors of $\pm 0.4\%$.[61] Calculations by Arenhoevel in the same reference predicted asymmetries of -0.33% and -0.24% , respectively. The small amount of time we request for Deuterium running is not for background subtraction. Rather, it is for exploratory measurements of P_N on the bound proton and neutron as discussed below in Section 3.7.

Although these nuclear backgrounds are expected to be negligible, we wish to emphasize that we have plenty of redundancy in their rejection. Once an electron is detected in the HMS and judged to be from elastic $e + p$ scattering because it falls within a narrow W cut, the conjugate proton angle is known except for minor, systematic steering by the solenoid. The fast tracking device located in front of the analyzing target will allow a cross-check on the proton angle to help suppress quasi-elastic scattering from the windows or shielding.

3.6 Trigger and Data Acquisition

An HMS *Electron* trigger would be ideal since it could introduce minimal bias in the polarimeter. However, this is not possible because at low Q^2 the elastic electron event rates are 10's of KHz which is beyond the capability of our data acquisition system. A coincidence is required with a polarimeter trigger which rejects most so-called "straight through" tracks for which there is no significant nuclear scattering in the CH_2 . The most elegant solution, which avoids the problem of extremely high rates in a veto scintillator, is a cylindrical barrel of scintillator which we call 2π .¹² The 2π barrel would encircle the proton beam downstream of the analyzing target, only detecting events which have scattered more than a few degrees, thus making

¹²The idea and the name are borrowed from a neutron polarimeter by John Watson.

it an excellent basis for the polarimeter trigger. The polarimeter singles trigger would therefore be *PolarimeterScatter* $\equiv S1 \cdot 2\pi$ and the experiment's primary trigger would be *Electron*·*PolarimeterScatter*. This will bring the coincidence rate down to the several KHz level, with event sizes no larger than standard HMS-SOS operations. Prescaled versions of high rate singles triggers such as HMS *Electron*, *PolarimeterScatter*, *S1*, and 2π would also be acquired.

3.7 Deuterium Measurements

In the $D(e, e'\vec{p})n$ reaction, P_N should be due to a combination of two-photon exchange effects and strong FSI. These two processes, however, have very different energy dependences, with the strong FSI effects decreasing with momentum transfer according to the calculations of Arenhoevel in reference [61], while the two-photon effects (loosely speaking) increase with energy. Unfortunately, the predictions for P_N in Deuterium are poorly tested, with the single point away from quasi-free kinematics lying somewhat over 2σ away from a calculation by Arenhoevel.[62]

The ideal way to disentangle these issues (*i.e.*, two-photon exchange versus strong FSI) is to measure P_N on both the free proton and the bound proton, with the proton measurement unambiguously providing the two-photon contribution. For Q^2 above 0.75 and θ_{CM} near 90° , if the two-photon contributions dominate as expected, then P_N measurements on the proton and deuteron should give similar values. If this could be demonstrated, then it would clearly be possible to measure two-photon contributions to P_N on the *neutron* via $D(e, e'\vec{n})p$.

For only our relatively high-rate kinematic settings, we have asked for 1/4 the Hydrogen running time for exploratory Deuterium measurements. This seems a small price in order to lay the groundwork for future neutron measurements. In the helicity amplitude formalism we have used to describe $e + p$ elastic scattering observables, the physics case for neutron measurements is not clear. However, that physics case will become clearer when theorists soon relate P_N to GPD's at higher Q^2 [63], and one tries to isolate the up- versus down- quark contributions.

3.7.1 Exploratory Measurements on the Neutron

Relative to proton polarimetry, we expect the figure of merit for neutron polarimetry to be competitive a low Q^2 (where thick analyzing targets can only be used for neutrons) and up to an order of magnitude lower at high Q^2 (where thick analyzing targets can be used for both protons and neutrons). This is because the (n, n) reactions are invisible, the (n, p) analyzing power at high energies is lower than the (p, p) analyzing power[64], and the efficiency for neutron detection in the rear detector is less than 100%. Using an active target, a feasibility measurement will be made at low Q^2 to look at backgrounds, etc.

3.8 Errors

We will discuss random errors separately from systematic errors. The error estimates are summarized in Table 4.

3.8.1 Random Errors

counting statistical errors

The counting statistical error on P_N is given by

$$\Delta P_N = \sqrt{\frac{2}{\text{effi} \langle A_Y \rangle^2 N}} \quad (29)$$

where *effi* is the efficiency for a useful scattering in the analyzing target, $\langle A_Y \rangle$ is the average effective analyzing power, and N is the total number of events. A useful quantity is the polarimeter figure of merit, or FOM, equal to $\text{effi} \langle A_Y \rangle^2$ which Punjabi *et al.*[49] found to be roughly 0.01. Our rates are calculated assuming this FOM and a simple dipole approximation to the proton form factors without radiative corrections.

additional statistical errors

The imperfect cancellation of long-term drifts (*e.g.*, in the Top-Bottom asymmetry due to a changing temperature gradient in wire chamber gas) will appear as an increase in the random error above counting statistics. One can search for such effects by performing the experiment and testing whether the asymmetry is converging to the final result $\propto 1/\sqrt{N}$. However, such effects are notoriously difficult to predict in advance of data-taking. We will assume such additional statistical errors are negligible but the price we must pay is frequent changes in proton precession angle. This results in significant experiment deadtime (20%), but we feel this is essential for an experiment of this type with 0.1% sensitivity.

3.8.2 Systematic Errors

uncertainty in the analyzing power, A_Y

An important systematic error will be the effective analyzing power. Although such an error of scale will not hide a non-zero physics asymmetry, if $\Delta P_N/P_N$ is larger than the statistical error, it will limit the interpretability of the measurement. Possible approaches are to either interpolate published $\langle A_Y(\theta) \rangle$ values on Carbon or to measure it directly using P_T .

Published values of the effective analyzing power of Carbon in proton polarimeters are available with few percent relative errors.[49] However, given the need to interpolate these results in proton energy, and even extrapolate in terms of slab thickness, a conservative error on the resulting $\langle A_Y \rangle$ for our kinematics and polarimeter would be 10%. For $P_N = 1\%$, this would produce a systematic error comparable with the statistical error. This is adequate for the experiment, but one

would prefer the error on $\langle A_Y \rangle$ to be negligible compared to the statistical errors. Also, CH_2 would not be an option as an analyzing target.

For this reason we plan to use the helicity-dependent transverse asymmetry, P_T ,

$$P_T = \frac{-2\sqrt{\tau(1+\tau)}G_E^p G_M^p \tan \theta_e/2}{(G_E^p)^2 + (\tau/\epsilon)(G_M^p)^2} \quad (30)$$

which is available for the additional experimental overhead of measuring the beam polarization and keeping track of the beam helicity in our data acquisition system. For the Q^2 range of this proposal, the uncertainty on P_T ranges from 1% to 5%.[49] Small corrections due to P_L will be needed, but this technique will allow $\langle A_Y \rangle$ to be determined with relative errors of 5% or better. This second approach assumes that the Hall A FPP data are correct. If they are incorrect, then the second method may yield a value for $\langle A_Y \rangle$ at $Q^2 = 1-2$ which is many σ different from the first method.

In summary, we expect the uncertainty due to $\langle A_Y \rangle$ will be less than 5%.

induced polarization by shielding window

Because left and right scatterings (or top and bottom) from the Lead window have opposite polarization, it is clear that for rescattering in the analyzing target to more than a few degrees there will be a high degree of cancellation. However, it is useful to estimate the magnitude of the polarization induced by the windows to see whether our experiment requires delicate cancellations of large induced polarizations.

An upper bound can quickly be placed on the polarization of protons caused by small angle nuclear scattering in the Lead window. This false asymmetry is less than $A_Y(\theta) \times \text{effi}$, where effi is the probability for undergoing an inelastic nuclear reaction which produces a proton at less than 1° . Assuming the window is located near the primary target, the acceptance of the polarimeter channel will only be about 1° . Many protons undergoing nuclear reactions will scatter to larger angles. Using the expressions $\text{effi} \ll 1\%N$ where N is the window thickness in g/cm^2 , and $A_Y = 0.6P \sin \theta$ for CH_2 [65] with the momentum P in units of GeV/c , then

$$A_{\text{window}} \ll 0.6P \sin \theta.01N \quad (31)$$

For the highest proton momentum in this proposal, 1.8 GeV/c , the asymmetry induced by the window is much less than 0.02% per g/cm^2 of window thickness. The effect of polarization induced by the Lead windows is therefore negligible for any reasonable window thickness.

uncertainty in the precession angle

From the formula for the precession angle

$$\chi = 51.1^\circ \frac{P}{M} \int B dL \quad (32)$$

one can see that systematic shifts in χ can arise from errors in the average nucleon momentum, P , and the average field integral $\int B dL$. Assuming the relative error on

the field integral $\int BdL$ is conservatively 1%, this is the dominant contribution to the systematic error on χ . (From two body kinematics, the average nucleon momentum is determined at the $O(0.1\%)$ -level from the electron arm angle and either the beam energy or the spectrometer momentum.) Therefore,

$$\Delta\chi \simeq 51.1^\circ \frac{P}{M} \Delta(\int BdL)$$

The worst case error is for the maximum precession angle, or $\Delta\chi = 1.8^\circ$ for $\chi = 180^\circ$. The resulting relative error on the asymmetry (and therefore P_N) is less than $1 - \cos(180^\circ - 1.8^\circ) = 0.05\%$ which is insignificant compared to the analyzing power. At the same precession angle, the *absolute* error on the false asymmetry in the orthogonal direction will be proportional to $P_N \sin(180^\circ - 1.8^\circ) = 0.03\%$. This is acceptably small, but if it were a factor of several larger it would dilute our sensitivity to P_N in fitting datasets such as that in Figure 13. This highlights the need for field integral measurements with relative errors of 1%.

residual χ -dependent errors

In this section, we only discuss χ -dependent false asymmetries which are not immediately resolved by minimizing stray magnetic fields or by using front-end tracking to correct the small steering changes. However, in all cases, these effects are either negligible, produce small effects proportional to χ or χ^2 which can be determined in a fit, or can be measured by modulating the beam in X-Y at 30 Hz.

Deadtime: Steering by the solenoid produces a change in the rate, and therefore deadtime, of channels in the 2π detector. If the detector is perfectly symmetric, or the deadtime is perfectly corrected, then no false asymmetry results. Errors in the deadtime correction appear as a false asymmetry, and shifts in these errors between χ and $\chi + 180^\circ$ will appear as a precession-dependent false asymmetry. For a 2π detector consisting of 16 bars at a combined maximum rate of 1 MHz, assuming an occupancy time of 25 nsec, the deadtime per bar is only about 0.16%. Even a crude correction for the deadtime will make it impossible for this to be a source of significant χ -dependent false asymmetries. This statement holds true even in the presence of a large background flux of highly polarized protons from inelastic reactions. Although the computer deadtime could be much higher (*e.g.* 20%) than the 2π detector, it doesn't appear that this can cause ϕ dependence leading to false asymmetries.

Tracking efficiency: We assume first that the front-end and rear tracking chambers have been well plateaued so that the efficiencies are not pathologically sensitive to path length variations. In the version of the analysis which uses the rear chambers to bin in ϕ, θ , tracking efficiency corrections may be needed to accommodate rate differences at different settings. Although the sensitivity of the tracking efficiency to beam steering will be easy to measure with X-Y modulating coils if it is large, it is difficult to estimate. For this reason we have specified a rather high efficiency of 98% for the rear tracking chamber.

Table 4: Summary of statistical and systematic errors on P_N for proton measurements.

| Errors | protons |
|----------------------------|---------------|
| Statistical: | |
| counting statistics | 0.0005-0.0025 |
| additional sources | $\simeq 0$ |
| Systematic: | |
| analyzing power | 5% |
| induced polarization | $\simeq 0$ |
| precession angle | $\simeq 0$ |
| differential absorption | $\simeq 0$ |
| rear tracking efficiency | 0.2% |
| (one analysis method only) | |

Differential Nuclear Absorption: Because the path length through the analyzing target will vary slightly with precession-dependent beam steering, differential nuclear absorption of protons can produce a precession-dependent false asymmetry. The effect is completely negligible except at large scattering angles in the analyzing target, where the figure of merit is nearly vanishing. At the scattering angle of 20° where there is still significant figure of merit, the path length differences are about 0.4%. Using the fact that the “disappearance” cross section is much smaller than the nuclear reaction cross section,

$$A_{absorption} \ll (0.004)(0.01N/2) \quad (33)$$

where N is the target thickness in g/cm^2 . For our thickest target of $40 g/cm^2$, $A_{absorption} \ll 0.08\%$, so this effect appears to be negligible.

projected errors

Projected errors for the lower two beam energies are shown in Figure 14 along with several independent predictions. This E_{CM} region is critical for understanding the role played by the Δ resonance. In the $N + \Delta$ calculation of Vanderhaeghen[63], destructive interference near 0.570 GeV beam energy causes P_N to essentially vanish and remain small at 0.855 GeV. This is not seen in the predictions of Guenter and Afanasev. The high precision of our proposed technique is a good match to the small size of the predicted asymmetries.

Projected errors for the higher beam energies are shown in figure 15. For E_{CM} well above the Δ resonance, only the calculation of Afanasev is available at this time. However, the model dependence of the inelastic contributions can be expected to be significant.

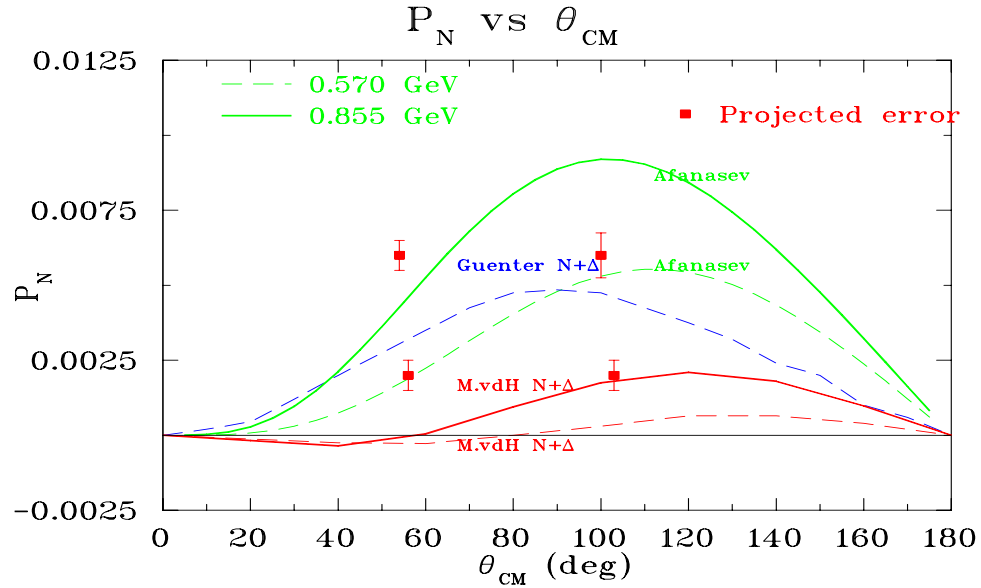


Figure 14: Projected statistical errors, plotted at arbitrary values of the asymmetry, for the two lowest beam energies we propose. A systematic uncertainty of 5% is to be understood. Several predictions for P_N highlight the model dependence of the inelastic contributions.

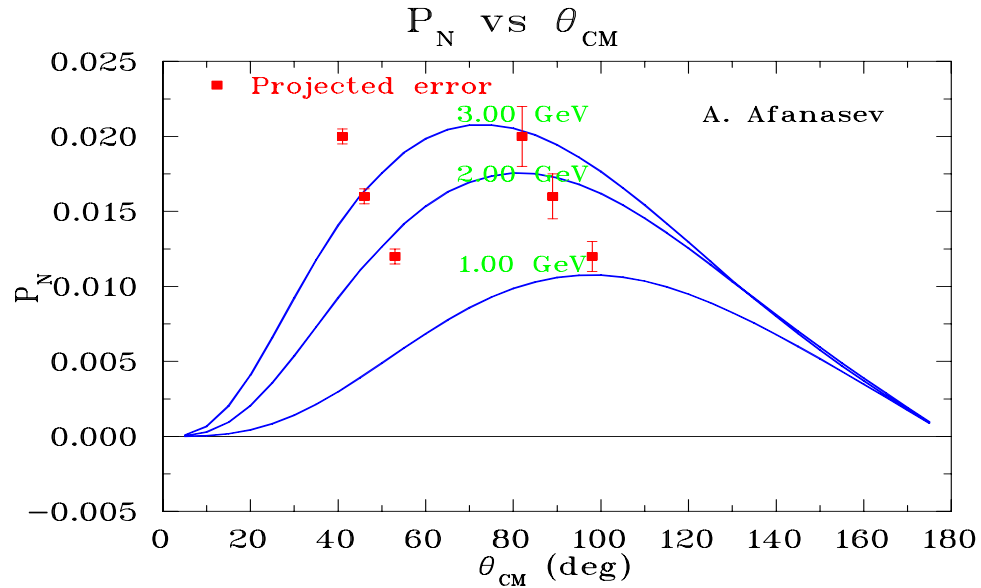


Figure 15: Projected statistical errors for the higher beam energies we propose. A systematic uncertainty of 5% is to be understood. Only the predictions of Afanasev are available at this large E_{CM} .

4 Relation to Other Experiments

JLab Proposal 98-102

Assamagan *et al.*[66] proposed at PAC14 to measure A_N in elastic, inelastic, and quasi-elastic scattering on a ${}^3\text{He}$ target polarized normal to the scattering plane. The experiment was rejected. This was unfortunate since the ${}^3\text{He}$ nucleus is a few body system, amenable to essentially exact calculations, and thus the experiment had the potential to make a definitive measurement of two-photon exchange effects in nuclei.

5 Collaboration

The collaboration consists of experts in:

- proton focal-plane polarimetry
- neutron polarimetry
- parity-conserving azimuthal beam asymmetries
- parity-violating asymmetries
- detector trigger and tracking technologies

All are motivated by high interest in the resolution of the “ G_E^p crisis” and the potential impact of box-diagram contributions on many classes of precision electroweak measurements.

Superconducting magnet refurbishment and stray field modelling will be done by the Hall C engineering and technical staff. The same Hall C engineering and technical staff has extensive experience mounting major installation experiments.

6 Beam Request

Our beam request is detailed in Table 5 at the end of this proposal. The Phase I request to this PAC is 27 days to measure P_N in ${}^1\text{H}(e, e'p)$ on Hydrogen, including exploratory measurements of P_N in $D(e, e'N)N_s$. The request is for polarized beam.

The allowable overhead was calculated as:

- 24 hours to set up 570 MeV, which is an unusually low energy for JLab
- For other energies: 8 hours for an energy change
- 4 hours per energy for a Moeller measurement at 2 microA
- 4 hours for angle change and realignment

- 2 hours to convert from proton to neutron running
- 0 hours for target changes

With a second solenoid, the experiment here could be extended to higher beam energies and momentum transfers where there is a link to the physics of GPD's. Depending on the outcome of our exploratory quasi-elastic measurements, there is also the possibility of extending these measurements to the neutron.

7 Acknowledgements

We would like to thank the following theory colleagues for pointing the way: Peter Blunden, Wally Melnitchouk, Michael Ramsey-Musolf, John Tjon, Marc Vanderhaeghen, and especially Andrei Afanasev. Chief Engineer Paul Brindza solved the stray field problems while driving TOSCA, and Designer Mike Fowler figured out how to cheaply change angles in CAD space.

References

- [1] Y.-S. Tsai, “Radiative Corrections to Electron-Proton Scattering”, Phys. Rev. **122**, 1898 (1961).
- [2] M.N. Rosenbluth, “High Energy Elastic Scattering of Electrons on Protons”, Phys. Rev. **79**, 615 (1950).
- [3] R. Hofstadter, “Electron Scattering and Nuclear Structure”, Reviews of Modern Physics **28** 214 (1956); R. Hofstadter *et al.*, “Electromagnetic Structure of the Proton and Neutron”, Reviews of Modern Physics **30** 482 (1958).
- [4] from N.R. Werthamer and M.A. Ruderman, “Nucleon Polarizability Correction to High-Energy Electron-Nucleon Scattering”, Phys. Rev. **123**, 1005 (1961), quoted with permission from APS and M.A. Ruderman.
- [5] A. Afanasev, private communication.
- [6] R. Arnold *et al.*, “Polarization Transfer in Elastic Electron Scattering from Nucleons and Deuterons”, Phys. Rev. C **23**, 363 (1981).
- [7] J. Arrington, private communication.
- [8] R. Gilman and L. Pentchev, private communication.
- [9] J. Mar *et al.*, “Comparison of Electron-Proton and Positron-Proton Elastic Scattering at Four-Momentum Transfers up to $5.0 (GeV/c)^2$ ”, Phys. Rev. Lett. **21**, 482 (1968); D. Yount and J. Pine, “Scattering of High-Energy Positrons from Protons”, Phys. Rev **128** 1842 (1962); A. Browman *et al.*, “Positron-Proton Scattering”, Phys. Rev. **139**, B1079 (1965); R.L. Anderson *et al.* “Positron-Proton Elastic Scattering at 800 and 1200 MeV”, Phys. Rev. **166**, 1336 (1968) (these results supersede the earlier results reported in *ibid*, Phys. Rev. Lett. **17** 407 (1966)); G. Cassiday *et al.*, “Comparison of Elastic Positron-Proton and Electron-Proton Scattering Cross Sections”, Phys. Rev. Lett. **19**, 1191 (1967).
- [10] S.P. Wells *et al.*, “Measurement of the vector analyzing power in elastic electron-proton scattering as a probe of the double virtual Compton amplitude”, Phys. Rev. C **63** 064001 (2001).
- [11] M. Jones *et al.*, “ G_E^p/G_M^p Ratio by $\vec{e} + p \rightarrow e + \vec{p}$ ”, Phys. Rev. Lett. **84**, 1398 (2000); O. Gayou *et al.*, “Measurements of the Elastic Electromagnetic Form Factor Ratio $\mu_p G_E^p/G_M^p$ via Polarization Transfer”, Phys. Rev. C **64**, 038202; O. Gayou *et al.*, “Measurement of G_E^p/G_M^p in $\vec{e} + p \rightarrow e + \vec{p}$ to $Q^2 = 5.6 GeV^2$ ”, Phys. Rev. Lett. **88**, 092301-1 (2002).

- [12] R. Segel and J. Arrington, private communication regarding preliminary results of JLab experiment Hall A experiment 01-001, “New Measurement of G_E/G_M for the Proton”.
- [13] A. Afanasev, “Radiative Corrections for Elastic Electron Proton Scattering”, Talk presented at the Workshop on Nucleno Form Factors and Parity Violation, October 2003, Athens, Greece.
- [14] R. Carlini *et al.* “The Q_{weak} Experiment: A Search for New Physics at the TeV Scale Via a Measurement of the Proton’s Weak Charge”, TJNAF proposal E-02-020
- [15] W.J. Marciano and A. Sirlin, “Radiative Corrections to Atomic Parity Violation”, Phys. Rev. D **27** 552 (1983).
- [16] W.J. Marciano and A. Sirlin, “Some general properties of the $O(\alpha)$ corrections to parity violation in atoms”, Phys. Rev. D **29**, 75 (1984).
- [17] J. Erler, A. Kurylov, and M.J. Ramsey-Musolf, “The Weak Charge of the Proton and New Physics”, Phys. Rev. D **68** 016006 (2003), and hep-ph/0302149v1 17Feb 2003.
- [18] A. Sirlin, Reviews of Modern Physics, **50** 573 (1978).
- [19] LANSCE proposal, “A proposal for an Accurate Measurement of the Neutron Spin - Electron Angular Correlation in Polarized Neutron Beta Decay with Ultracold Neutrons”, T. Bowles and A.R. Young, 2000; downloadable from <http://www.krl.caltech.edu/ucn/physics.html>
- [20] J. Gunion and Leo Stodolsky, “Two-Photon Exchange in Electron-Deuteron Scattering”, Phys. Rev. Lett. **30**, 345 (1973).
- [21] V. Franco, “Electron-Deuteron Scattering and Two-Photon Exchange”, Phys. Rev. D **8**, 826 (1973).
- [22] M.P. Rekalo *et al.*, “Search for evidence of two-photon exchange in new experimental high momentum transfer data on electron deuteron elastic scattering”, Phys. Rev. C **60**, 042202 (1999).
- [23] E.A.J.M. Offermann *et al.*, “Energy Dependence of the Form Factor for Elastic Electron Scattering from ^{12}C ”, Phys. Rev. C **44**, 1096 (1991), and references therein.
- [24] A. DeRujula *et al.*, “Elastic Scattering of Electrons from Polarized Protons and Inelastic Electron Scattering Experiments”, Nuclear Physics **B35** 365 (1971).

- [25] S.D. Drell and M.A. Ruderman, "Proton Polarizability Correction to Electron-Proton Scattering", Phys. Rev. **106**, 561 (1957); and S.D. Drell and S. Fubini, "Higher Electromagnetic Corrections to Electron-Proton Scattering", Phys. Rev. **113**, 741 (1959).
- [26] S. Wells, private communication.
- [27] G.K. Greenhut, "Two-Photon Exchange in Electron-Proton Scattering", Phys. Rev. **184**, 1860 (1969).
- [28] J. Mar *et al.*, "Comparison of Electron-Proton and Positron-Proton Elastic Scattering at Four-Momentum Transfers up to $5.0 (GeV/c)^2$ ", Phys. Rev. Lett. **21**, 482 (1968).
- [29] D.L. Fancher *et al.*, "Precision Comparison of Inelastic Electron and Positron Scattering from Hydrogen", Phys. Rev. Lett. **37**, 1323 (1976).
- [30] A. Afanasev, I. Akushevish, and N.P. Merenkov, "Nucleon Compton Scattering with Two Space-like Photons", hep-ph/0208260 v1 28 Aug 2002.
- [31] J.C. Bizot *et al.* "Measurement of the Polarization of Recoil Protons from $e - p$ Scattering at 950 MeV", Phys. Rev. Lett. **11**, 480 (1963); *ibid*, "Polarization of Recoil Protons from Electron-Proton Scattering at 950 MeV", Phys. Rev. **140**, B1387 (1965).
- [32] G.V. Di Giorgio *et al.*, "Polarization of Recoil Protons in e-p Elastic Scattering at 20 fermi⁻²", Il Nuovo Cimento, **39**,474 (1965).
- [33] D.E. Lundquist *et al.*, "Polarization of Recoil Protons from Neutral Pion Photoproduction", Phys. Rev. **168**, 1527 (1968). (The elastic results are on page 1531.)
- [34] R. Prepost, R.M. Simonds, and B.H. Wiik, "Test of Time-Reversal Invariance in Elastic Electron Scattering From the Deuteron", Phys. Rev. Lett. **21**, 1271 (1968).
- [35] J. Bernstein, G. Feinberg, and T.D. Lee, "Possible C,T Noninvariance in the Electromagnetic Interaction", Phys. Rev. **139**, B1650 (1965).
- [36] N. Christ and T.D. Lee, "Possible Tests of C_{st} and T_{st} Invariances in $l^\pm + N \rightarrow l^\pm + \Upsilon$ and $A \rightarrow B + e^+ + e^-$ ", Phys. Rev. **143**, 1310 (1966).
- [37] S. Rock *et al.*, "Search for T-Invariance Violation in the Inelastic Scattering of Electrons from a Polarized Proton Target", Phys. Rev. Lett. **24**, 748 (1970).
- [38] G. Feinberg and H.S. Mani, Phys. Rev. **137**, B636 (1965).

- [39] G. Feinberg, “Some Consequences of the Proposed C and T Violations in Electromagnetic Interactions”, *Phys. Rev.* **140**, B1402 (1965).
- [40] T. Powell *et al.*, “Measurement of the Polarization in Elastic Electron-Proton Scattering”, *Phys. Rev. Lett.* **24**, 753 (1970).
- [41] F. Guerin and C.A. Picketty, “Polarization Effects in Elastic Lepton-Proton Electromagnetic Scattering”, *Il Nuovo Cimento*, **32** 971 (1964).
- [42] J. Arafune and Y. Shimizu, “Proton Polarization in Elastic Electron-Proton Scattering”, *Phys. Rev. D* **1**, 3094 (1970).
- [43] U. Guenter and R. Rodenberg, “Polarization of the Recoil Protons in the Elastic Electron-Proton Scattering Process”, *Il Nuovo Cimento* **2A** 25 (1971).
- [44] J.R. Chen *et al.* “Test of Time-Reversal Invariance in Electroproduction Interactions Using a Polarized Proton Target”, *Phys. Rev. Lett.* **21** 1279 (1968).
- [45] A. Afanasev, private communication.
- [46] P.G. Blunden, W. Melnitchouk, and J.A. Tjon, “Two-photon exchange and elastic electron-proton scattering”, *nucl-th/0306076v1* 25Jun 2003.
- [47] M. Palarczyk *et al.*, “INPOL - the Indiana University Neutron Polarimeter”, *Nuc. Instr. Methods* **A457** (2001) 309-331, and references therein.
- [48] T.N. Taddeucci *et al.*, “A Neutron Polarimeter for (p, n) Measurements at Intermediate Energies”, *Nuc. Instr. Methods* **A241** (1985) 448-460.
- [49] V. Punjabi *et al.* “Proton Elastic Form Factor Ratios to $Q^2 = 3.5 \text{ GeV}^2$ by Polarization Transfer”, submitted to *Phys. Rev. C*.
- [50] TJNAF Proposal, “Measurement of G_E^p/G_M^p to $Q^2 = 9 \text{ GeV}^2$ via Recoil Polarization”, C.F. Perdrisat *et al.*
- [51] Frank Maas, private communication.
- [52] F.E. Maas for the A4 Collaboration, “Two Photon Physics in Elastic Electron Scattering: Experimental Status”, talk presented at Trento, April 4, 2003.
- [53] P. Brindza, Hall C Chief Engineer (and TOSCA driver), private communication.
- [54] S. Danagoulian, private communication.
- [55] Eljen Technology, <http://www.apace-science.com/eljen/index.htm>
- [56] Saint-Gobain, <http://www.detectors.saint-gobain.com>

- [57] E. Korkmaz *et al.*, “Segmented Detector for Recoil Neutrons in the $p(\gamma, n)\pi^+$ reaction”, NIM **A431** (1999) 446-454.
- [58] Steve Wood, private communication.
- [59] J. Rapaport, T. Rinckel, and J. Vanderwerp, private communications; also email from Roger Wheatley (AMI Magnet Division Manager) to Paul Brindza.
- [60] R.J. Woo *et al.*, “Measurement of the Induced Proton Polarization P_N in the $^{12}\text{C}(e, e'\bar{p})$ Reaction” , Phys. Rev. Lett. **80** 456 (1998).
- [61] B.D. Milbrath *et al.*, “Comparison of Polarization Observables in Electron Scattering from the Proton and Deuteron”, Phys. Rev. Lett. **80** 452 (1998).
- [62] D. Barkhuff *et al.*, “Measurement of Recoil Proton Polarizations in the Electrodisintegration of Deuterium by Polarized Electrons”, Phys. Lett. B **470** 39 (1999).
- [63] M. Vanderhaeghen, private communication.
- [64] R. Diebold *et al.*, “Measurement of the Proton-Neutron Elastic-Scattering Polarization from 2 to 6 GeV/c”, Phys. Rev. Lett. **35** 632 (1975).
- [65] C.F. Perdrisat *et al.*, Proposal to PAC20, “Measurement of G_E^p/G_M^p to $Q^2 = 9 \text{ GeV}^2$ via Recoil Polarization”.
- [66] K. Assamagan *et al.*, “A Measurement of Dispersive Effects in the Elastic and Inelastic Scattering of Electrons from ^3He ”, JLab proposal PR98-102.

A Neutron Polarimetry

Because neutrons are not charged, they only make their presence known when they undergo reactions which transfer energy to charged particles. The scattering angle is measured with respect to two lines: one line from the target center to a hit in the active target, and a second line from the active target hit to a hit in a rear detector. At intermediate energies, the most important reaction is $n + p$ elastic scattering to small angles because it has a relatively high cross section, a high analyzing power, and is detectable in an active analyzing target if the recoil proton has sufficient energy. (The reaction $n + n$ produces few charged products and plays little role.) Compared to proton polarimetry, neutron polarimetry is more sensitive to neutral backgrounds, an active target is essential, scattering angle determination is crude but adequate, and the rear detector must be quite massive in order to have high efficiency and to cover the necessary solid angle.

A coincidence between a good quasi-elastic electron in the HMS and a neutral in the active target ($HMS \cdot T2neutral$) allows one to define the incident neutron flux N_0 in a manner which is insensitive to neutral backgrounds and stable with time. The normalized scattered azimuthal distribution, $N(\phi)/N_0$, is then used to determine the azimuthal asymmetry. Fortunately, there is no Coulomb multiple scattering for neutrons, hence the analyzing target can be up to a large fraction of a nuclear reaction length even at low energies. This is helpful in gaining back the efficiency lost due to the “invisible” (n, n) reactions.

Most of the protons in a CH_2 target are bound in Carbon, so it is not surprising that a large fraction of the events have small analyzing power due to complex, non-quasifree reactions. In fact, cuts are normally used to optimize the figure of merit in neutron polarimetry.[48] Two sets of cuts enhance the high-analyzing-power $n + p$ (quasi-)elastic scattering reaction: the first is to require the expected correlation between the neutron scattering angle and the recoil energy measured in the active target; the second is to require that the scattered neutron have the expected velocity during flight between the active target and the rear detector. A fortunate side-effect of these cuts is to help suppress low energy neutral backgrounds. Pulse-shape discrimination to specifically suppress γ ray backgrounds would also be of benefit.[57] Since analyzing power is not an issue in the rear detector, we will employ a liquid scintillator with optimal pulse-shape discrimination properties. The rear bars will be digitized by flash ADC’s so that the pulse shape discrimination can be optimized offline.

The dimensions of the active target will be a fairly compact: 30 cm x 30 cm frontal area, and with thickness of 36 cm. It will consist of a mineral-oil based scintillator[55, 56] with a high C:H ratio of 1:2. Two designs are being considered: one is completely straightforward and the other involves significant R&D. The conservative design calls for loading the liquid scintillator into thin-walled stainless steel vessels of dimension, 3 cm x 6 cm x 30 cm, with 10 per layer. Dividing the active area into 10 channels of 3 cm pitch is important because it reduces the deadtime

per channel as well as the probability that a neutral event will be vetoed by an unrelated charged track. Alternate layers will have the bars oriented horizontally and vertically. Two layers will make a “block” of 12 cm thickness. Active target thicknesses can be 12 cm, 24 cm, and 36 cm. All neutron running will use 36 cm thickness.

Each bar will have a short lightguide and a 1” pmt on each end, yielding a total of 120 pmt’s. Because the bars are mean-timed in software, short, and only 6 cm thick, timing resolution will be good even for neutrons. Pulse height resolution will also be excellent. These are useful qualities for improving the figure of merit offline with cuts.

Table 5: Phase I beam request for the various settings. At each setting, the proton polarization will be precessed in steps of 90 degrees. The time request for Deuterium running is 1/4 that of the Hydrogen time, and will be used for both proton and neutron measurements. The analyzing target thickness is chosen to provide a maximum of 0.9° of multiple scattering, subject to a maximum thickness of 40 cm.

| ID | E_e (GeV) | E_{CM} (GeV) | θ_{CM} (deg) | Lum. cm^2/sec | CH_2 Thick. (cm) | Elastic Rate (KHz) | dA_N (stat) | Beam Time (hrs) | Overhead (hrs) |
|----------|----------------|-------------------|------------------------|--------------------|--------------------------|--------------------------|------------------|-----------------------|-------------------|
| 1a H | .570 | 1.40 | 102.7 | 510^{37} | 6.9 | 9.56 | .0005 | 58.1 | 28. |
| D | | | | | | | .001 | 14.5 | 2. |
| 1b H | | | 56.3 | 10^{37} | 1.0 | 31.7 | .0005 | 8.8 | 4. |
| D | | | | | | | .001 | 2.2 | 2. |
| 2a H | .855 | 1.58 | 99.8 | 510^{37} | 18. | 3.65 | .001 | 67.6 | 16. |
| D | | | | | | | .002 | 16.9 | 2. |
| 2b H | | | 53.8 | 10^{37} | 2.6 | 20.6 | .0005 | 13.5 | 4. |
| D | | | | | | | .001 | 3.4 | 2. |
| 3a H | 1.00 | 1.66 | 98.4 | 510^{37} | 25. | 2.51 | .0015 | 55.3 | 16. |
| 3b H | | | 52.6 | 10^{37} | 3.6 | 18.0 | .0005 | 15.5 | 4. |
| D | | | | | | | .001 | 3.9 | 2. |
| 4a H | 2.00 | 2.15 | 89.4 | 510^{37} | 40. | .577 | .002 | 107. | 16. |
| 4b H | | | 45.9 | 10^{37} | 11. | 12.5 | .0005 | 22.3 | 4. |
| D | | | | | | | .001 | 5.6 | 2. |
| 5a H | 3.00 | 2.55 | 82.4 | 510^{37} | 40. | .321 | .0025 | 108. | 16. |
| 5b H | | | 41.0 | 10^{37} | 17.5 | 12.7 | .0005 | 21.9 | 4. |
| D | | | | | | | .001 | 5.5 | 2. |
| subtotal | | | | | | | | 530 | 126 |
| Total | | | | | | | | | 656 |